LETTERS
https://doi.org/10.1038/s42255-021-00410-x
nature metabolism

Check for updates

Elevated dietary ω-6 polyunsaturated fatty acids induce reversible peripheral nerve dysfunction that exacerbates comorbid pain conditions

Jacob T. Boyd[1,4], Peter M. LoCoco[1,4], Ashley R. Furr[1], Michelle R. Bendele[1], Meilinn Tram[1], Qun Li[1], Fang-Mei Chang[1], Madeline E. Colley[2], Grace M. Samenuk[2], Dominic A. Arris[1], Erin E. Locke[1], Stephan B. H. Bach[2], Alejandro Tobon[3], Shivani B. Ruparel[1] and Kenneth M. Hargreaves[1]✉

Chronic pain is the leading cause of disability worldwide[1] and is commonly associated with comorbid disorders[2]. However, the role of diet in chronic pain is poorly understood. Of particular interest is the Western-style diet, enriched with ω-6 polyunsaturated fatty acids (PUFAs) that accumulate in membrane phospholipids and oxidise into pronociceptive oxylipins[3,4]. Here we report that mice administered an ω-6 PUFA-enriched diet develop persistent nociceptive hypersensitivities, spontaneously active and hyper-responsive glabrous afferent fibres and histologic markers of peripheral nerve damage reminiscent of a peripheral neuropathy. Linoleic and arachidonic acids accumulate in lumbar dorsal root ganglia, with increased liberation via elevated phospholipase (PLA)2 activity. Pharmacological and molecular inhibition of PLA2G7 or diet reversal with high levels of ω-3 PUFAs attenuate nociceptive behaviours, neurophysiologic abnormalities and afferent histopathology induced by high ω-6 intake. Additionally, ω-6 PUFA accumulation exacerbates allodynia observed in preclinical inflammatory and neuropathic pain models and is strongly correlated with multiple pain indices of clinical diabetic neuropathy. Collectively, these data reveal dietary enrichment with ω-6 PUFAs as a new aetiology of peripheral neuropathy and risk factor for chronic pain and implicate multiple therapeutic considerations for clinical pain management.

Although medical recommendations about diet are made for cardiovascular disease[5], diabetes[6] and autoimmune diseases[7], this is not the case for most pain disorders. Poor nutrition certainly could be a risk factor for chronic pain conditions, especially with excess intake of ω-6 PUFAs, including linoleic acid (LA) and arachidonic acid (AA). Cellular membrane levels of these essential fatty acids are regulated by dietary intake and necessitate ~1% of total calories. The average daily Western diet, however, contains 10–20-fold greater ω-6 PUFA levels[8,9]. This discrepancy may have considerable clinical importance as ω-6 PUFAs undergo oxidation into pronociceptive oxylipins[10–14]. Elevated ω-6 levels are associated with pain conditions such as irritable bowel syndrome[15], rheumatoid arthritis[16] and headache[17]. Therefore, we evaluated the role of dietary ω-6 PUFAs in the development of persistent pain.

To determine whether elevated dietary ω-6 PUFAs affect nociceptive thresholds, we administered either a diet high in ω-6 PUFAs (H6D) composed of 11.8% kcal per kg ω-6 PUFAs or an isocaloric diet low in ω-6 PUFAs (L6D) composed of 0.4% kcal per kg ω-6 PUFAs to male and female mice for 24 weeks (Supplementary Table 1). Strikingly, both males and females on the H6D developed persistent hypersensitivity to mechanical and heat stimulation, which peaked at 8 weeks (Extended Data Fig. 1). Additional testing at 8 weeks revealed that mice fed the H6D exhibited mechanical hypersensitivity across a range of stimulus intensities, including dynamic brush-evoked stimulation (Fig. 1a,b). H6D-fed mice also demonstrated hypersensitivity to noxious cold and heat (Fig. 1c,d). Saturated fatty acid (SFA) content but not monounsaturated or ω-3 PUFA levels was modified to compensate for the different ω-6 PUFA levels in each diet (Supplementary Table 1). As SFAs can affect physical properties of cell membranes, it is possible that changes in dietary content could contribute to the observed phenotype. However, before receiving the L6D or the H6D, mice were maintained on a standard chow diet (2.9% ω-6 PUFA levels, 0.8% SFA levels) and exhibited behavioural responses that were indistinguishable from responses of mice on the L6D (Extended Data Fig. 1).

We performed single-fibre electrophysiologic recordings from ex vivo glabrous skin–tibial nerve preparations to characterise the effect of the H6D after 8 weeks on detection and firing properties of peripheral afferent fibres. Interestingly, we found that 40.9% of recorded fibres from mice fed the H6D exhibited spontaneous firing as compared to only 5.8% of those in mice fed the L6D (Fig. 1e,f). The H6D increased mechanical-evoked activity in C and A fibres as well as post-stimulus afterdischarge (Fig. 1g,h and Extended Data Fig. 2a,b). Moreover, using a Peltier thermal delivery system, we determined that heat-activated fibres from mice fed the H6D had reduced activation thresholds, increased firing frequency and prolonged post-stimulus activity (Fig. 1i,j and Extended Data Fig. 2c). Conduction velocities for both C and AM fibres were unchanged between diet groups (Extended Data Fig. 2d). Overall, the H6D-induced hyper-responsiveness of afferent fibres to mechanical and heat stimuli parallels mechanical- and heat-evoked hypersensitivities observed behaviourally in the same plantar hindpaw tissue.

We subsequently evaluated histologic markers of peripheral nerve damage to determine the presence of diet-induced neuronal damage. Mice fed the H6D exhibited a significant reduction in intraepidermal nerve fibre (IENF) density, an established marker of preclinical and clinical peripheral neuropathy[18,19], in glabrous skin after 8 weeks on the diet (Fig. 1k and Extended Data Fig. 2e).

[1]Department of Endodontics, University of Texas Health Science Center at San Antonio, San Antonio, TX, USA. [2]Department of Chemistry, University of Texas San Antonio, San Antonio, TX, USA. [3]Department of Neurology, South Texas Veterans Health Care System, San Antonio, TX, USA. [4]These authors contributed equally: Jacob T. Boyd, Peter M. LoCoco. ✉e-mail: hargreaves@uthscsa.edu

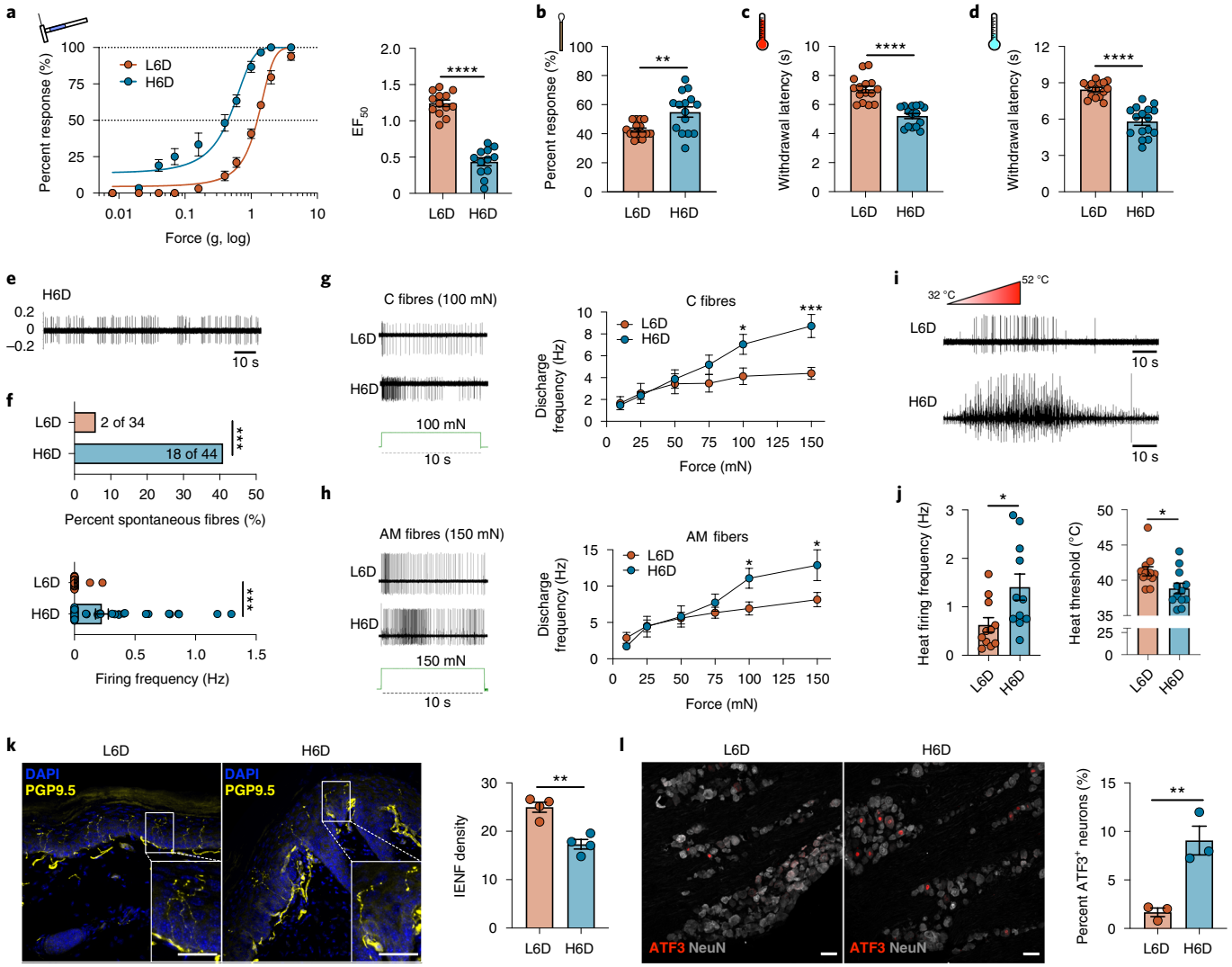

Fig. 1 | An ω-6 fatty acid-enriched diet induces a peripheral neuropathy–like phenotype in mice. a–d, Effects of a high 11.8% ω-6 fatty acid diet (H6D) or a low 0.4% ω-6 fatty acid diet (L6D) on nociceptive thresholds after 8 weeks. **a**, Mechanical force–response curves (left) and half-maximal effective force (EF_{50}) values (right) as determined with nonlinear regression (mice fed the L6D, $n=13$; mice fed the H6D, $n=12$). $^{****}P<0.0001$. **b**, Responsiveness to dynamic brush stimulation (L6D, $n=16$; H6D, $n=15$). $^{**}P=0.0022$. **c**,**d**, Paw-withdrawal latencies (s) in response to radiant heat (**c**) and cold (**d**) stimulation (L6D, $n=15$; H6D, $n=16$). $^{****}P<0.0001$ (**c**,**d**). **e**–**j**, Effects of diet on neurophysiologic firing properties of mouse glabrous afferent fibres. **e**, Representative recording of spontaneous firing activity from a mouse fed the H6D after 8 weeks. **f**, Percentage of spontaneously active fibres with discharge frequencies (L6D, $n=34$; H6D, $n=44$). $^{***}P=0.0005$ (top), $^{***}P=0.0006$ (bottom). **g**,**h**, Representative firing activities of C fibres (**g**) and AM fibres (**h**) responding to 100-mN and 150-mN square force stimulation for 10 s (in green), respectively. Discharge frequencies for each force tested are to the right for each fibre subtype (L6D, C fibres, $n=14$; H6D, C fibres, $n=13$; L6D, AM fibres, $n=23$; H6D, AM fibres, $n=12$). $^{***}P=0.0007$ (**g**), $^{*}P=0.0432$ (**g**), $^{*}P=0.0387$ (**h**, 100 mN), 0.0288 (**h**, 150 mN). **i**, Representative firing activities during a heat ramp. **j**, Discharge frequencies (left) and heat thresholds (right) of heat-responsive fibres (L6D, $n=12$; H6D, $n=12$). $^{*}P=0.0204$ (left), $^{*}P=0.0213$ (right). **k**, Representative immunofluorescence staining of hydrolase PGP9.5 (yellow) with 4,6-diamidino-2-phenylindole (DAPI) (blue) to visualise IENFs in glabrous hindpaw skin; scale bar, 50 µm. Insets, designated boxed regions magnified 2.5 fold; scale bar, 25 µm. IENF densities (right, L6D, $n=4$; H6D, $n=4$). $^{**}P=0.0018$. **l**, Representative immunofluorescence staining of ATF3 (red) expression in $NeuN^{+}$ lumbar DRG perikarya (grey); scale bar, 50 µm. Percentage of $ATF3^{+}$ neurons (right, L6D, $n=3$; H6D, $n=3$). $^{**}P=0.0087$. Data were collected from mice after 8 weeks on the respective diet. All data are mean ± s.e.m. Error bars may be within the size of the symbol. Statistical tests used were unpaired two-tailed Student's *t*-test (**a**–**d**, **f** (bottom), **j**–**l**), two-sided Fisher's exact test (**f**, top) and two-way ANOVA with Sidak's post hoc test (**g**,**h**).

More perikarya from dorsal root ganglia (DRG) as well as trigeminal ganglia from mice fed the H6D expressed the neuronal stress marker NeuN and activating transcription factor 3 (ATF3)[20,21] compared to those from mice fed the L6D for at least 8 weeks (Fig. 1l and Extended Data Fig. 2f,g). By contrast, immunolabelling of the lumbar spinal cord with IBA1 and c-FOS, markers for microglial and spinal neuron activation, respectively, was not different between groups (Extended Data Fig. 2h,i). Together, the reduction in glabrous IENF density and upregulation of ATF3 in DRG and trigeminal ganglia demonstrate the onset of peripheral nerve damage in mice within 8 weeks on the H6D. In total, behavioural, neurophysiologic and pathohistologic data indicate that mice quickly develop a peripheral neuropathy–like phenotype when fed an ω-6 PUFA-enriched Western-style diet.

Given that high-fat diet consumption is commonly associated with dyslipidaemia, insulin insensitivity and glucose dysregulation[22–26], we tested whether the H6D triggered onset of diabetes and subsequent neuropathy. Blood glucose and haemoglobin (Hb)A1c levels from mice fed the H6D were comparable to those of mice given the L6D or normal chow, while db/db diabetic mice exhibited elevated levels of both (Extended Data Fig. 3a,b). Additionally, weekly food consumption and body weights in mice fed the H6D were no different than those observed in mice fed the L6D (Extended Data Fig. 3c,d). Therefore, the observed neuropathy-like phenotype does not result from the induction of diabetes.

Rats previously given an H6D showed LA and AA accumulation in multiple tissues, including the brain[27]. As diet-induced nociceptive behaviours can be peripherally and/or centrally mediated[13,28–31], we next evaluated changes in lipid composition for lumbar DRG and spinal cords of mice fed the H6D after 8 weeks using unbiased shotgun lipidomics. Striking changes were observed across lipid classes in lumbar DRG but not spinal cords for both male and female mice fed the H6D compared to those in mice fed the L6D (Extended Data Fig. 4a,b). We quantified total ω-6 lipids in each tissue and found that both LA and AA levels were elevated but only in DRG from mice fed the H6D (Fig. 2a,b). Subprofiling revealed non-uniform accumulation of LA and AA across lipid classes, with robust increases among membrane-associated lipids, whereas ω-3 PUFAs remained largely unchanged (Extended Data Fig. 4c,d). Interestingly, we observed marked increases in lysophospholipid levels in DRG of mice fed the H6D (Fig. 2c). Lysophospholipids arise in abundance following enzymatic cleavage of *sn*-2 fatty acids by PLA2 enzymes and are known to be elevated in diabetes, coronary heart disease[32] and even neuropathic pain[33]. The release of *sn*-2-localised LA and AA from membrane phospholipids by PLA2 initiates their conversion into oxidised, pronociceptive metabolites[34]. Thus, we hypothesised that increased release of ω-6 fatty acids by PLA2 in DRG neurons elevates production of pronociceptive metabolites that underlie the H6D-associated neuropathic phenotype.

Expression and activity of PLA2 isozymes govern the release of membrane phospholipid-bound LA and AA[35]. We first assessed whether the H6D altered *Pla2* isozyme expression in lumbar DRG. Previous single-cell RNA-sequencing identified *Pla2g7* as the most prominent isoform in lumbar DRG neurons[36], accounting for 70–90% of *Pla2* transcripts across all sensory neuron subclasses (Extended Data Fig. 5a). We replicated these findings with quantitative (q)PCR using whole-DRG RNA extracts as well as by immunolabelling PLA2G7 expression across established afferent neuron subclasses (Extended Data Fig. 5b–e). Surprisingly, expression of *Pla2g7* and other prominent isozymes was unchanged in DRG from H6D-fed mice (Fig. 2d). Circulating PLA2G7 levels also were not different between L6D- and H6D-fed mice, despite increased LA levels in plasma from H6D-fed mice (Extended Data Fig. 5f,g). As the H6D did not alter PLA2 expression, we proceeded to evaluate changes in activity.

A recent clinical trial reported increased plasma PLA2G7 activity in patients on an 8-week LA-rich diet[37]. Thus, we investigated changes in PLA2 activity from afferent neurons from H6D-fed mice by exposing purified DRG homogenates to a phospholipid reporter containing dual fluorogenic boron dipyrromethene (BODIPY) acyl chains (Fig. 2e). DRG homogenates from H6D-fed mice exhibited greater fluorescence output compared to those from L6D-fed mice, indicating elevated PLA2 activity (Fig. 2f and Extended Data Fig. 6a). Expression of annexins, established repressors of PLA2 activity, in DRG from H6D-fed mice was unchanged (Extended Data Fig. 6b). However, there was an accumulation of PLA2G7 protein in the cytosolic fraction of DRG homogenates from H6D-fed mice, implicating an H6D-induced change in intracellular PLA2G7 turnover (Extended Data Fig. 6c).

To assess the contribution of PLA2G7, DRG lysates were pre-incubated with the selective inhibitor darapladib[38] before BODIPY exposure. PLA2 activity was reduced in a concentration-dependent manner, with 80% maximal inhibition, suggesting that PLA2G7 mediates the majority of PLA2 activity in DRG (Fig. 2f and Extended Data Fig. 6d,e). Lipidomics showed that ω-6 lipids accumulate in the glabrous skin of H6D-fed mice, similar to DRG (Extended Data Fig. 6f). Therefore, we next tested whether inhibition of PLA2G7 in glabrous skin attenuates H6D-induced nociceptive behaviours. Administration of a local, intraplantar injection of darapladib dose dependently reversed both heat and mechanical hypersensitivity in H6D-fed mice (Fig. 2g and Extended Data Fig. 6g). To validate selective inhibition of PLA2G7 with darapladib, we administered intrathecally (i.t.) *Pla2g7*-directed small interfering (si)RNA, which reduced *Pla2g7* expression in DRG and the spinal cord (Extended Data Fig. 6h,i). As with darapladib, *Pla2g7* knockdown reversed H6D-induced heat and mechanical hypersensitivities, whereas no effect was observed with scrambled siRNA (Fig. 2h). Glabrous IENF density was unaffected by siRNA treatment (Extended Data Fig. 6j). *Pla2g7* siRNA reduced transcript expression in L6D-fed mice, but no effect was observed behaviourally. To further link elevated ω-6 PUFA release to nociceptive hypersensitivity, darapladib and *Pla2g7* siRNA treatments were tested on db/db mice, and both attenuated the observed mechanical allodynia (Extended Data Fig. 6k–n). These collective data indicate that blocking oxylipin generation through inhibition of the predominant PLA2 isozyme in lumbar DRG is sufficient to reverse H6D-induced hypersensitivity.

As blocking PLA2-mediated lipid release reversed hypersensitivity, we next tested whether balancing lipid membrane content through dietary intervention would also reverse the phenotype. It is well documented that ω-3 PUFA oxylipins exhibit anti-inflammatory and anti-nociceptive effects, which directly counter pro-inflammatory, pronociceptive effects caused by oxidised ω-6 metabolites[39–41]. It is unclear, however, whether re-establishing the ω-6–ω-3 balance with diet could reverse the H6D-induced neuropathy phenotype. To test this, mice were fed the H6D for 8 weeks, at which point they were switched to a diet high in ω-3 PUFA (H3D) or the L6D or continued on the H6D for another 8 weeks (Fig. 3a and Supplementary Table 1). Mice given the L6D demonstrated marginally improved nociceptive thresholds compared to H6D-fed mice, whereas switching to the H3D completely rescued behavioural hypersensitivities (Fig. 3b,c). H3D-fed mice exhibited fewer spontaneously active glabrous afferent fibres, and both C and A fibres demonstrated recoveries in mechanical responsiveness, post-stimulus afterdischarge and heat thresholds (Fig. 3d–g and Extended Data Fig. 7a,b). H3D IENF densities and DRG ATF3 expression recovered relative to historical levels in mice on the L6D (Fig. 3h,i and Extended Data Fig. 7c,d). Furthermore, LA levels and PLA2 activity in DRG of H3D-fed mice were reduced (Fig. 3j,k). In sum, switching to the H3D rescued behavioural, electrophysiologic, pathohistologic and metabolic alterations associated with the H6D-induced neuropathy phenotype.

Despite the translational potential here, patients struggle to implement dietary and behavioural changes into their daily routines[42]. Nutritional supplementation may represent a more practical alternative to daily regulation of dietary PUFAs. To investigate this, mice were placed on the H6D for 8 weeks and then began receiving a daily ω-6 or ω-3 fatty acid supplement via gavage while also continuing the H6D (Fig. 3l). Interestingly, after 4 weeks of gavage, mice receiving the ω-3 fatty acid supplement exhibited partial recoveries of their pre-H6D nociceptive thresholds (Fig. 3m,n). Continued supplementation maintained these recoveries for the final 4 weeks of testing. These ω-3 fatty acid–supplementation data, along with H3D reversal data, indicate that both increasing ω-3 fatty acid

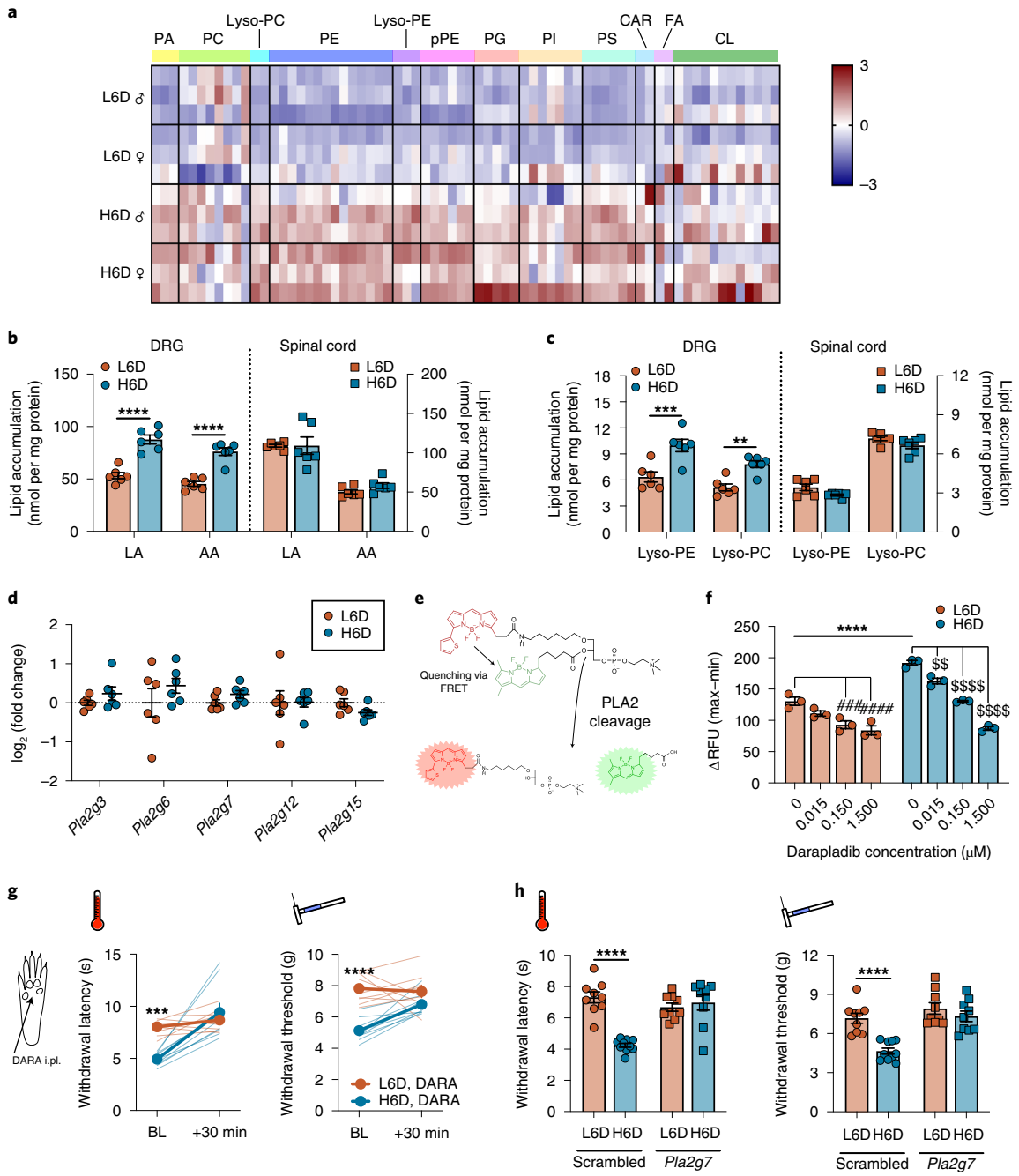

Fig. 2 | The H6D increases membrane loading of ω-6 PUFAs and stimulates PLA2 activity in peripheral afferent neurons. a, Heatmap of LA- and AA-esterified lipid species in lumbar DRG from male (♂) and female (♀) mice on either diet. Lipid classes are designated above the heatmap. The scale bar represents *z*-score transformations for each lipid species ($n=3$ mice per sex per diet). CL, cardiolipin; FA, fatty acid; lyso-PC, lysophosphatidylcholine; lyso-PE; lysophosphatidylethanolamine; PA, phosphatidic acid; PC, phosphatidylcholine; PE, phosphatidylethanolamine; PG, phosphatidylglycerol; PI, phosphatidylinositol; PS, phosphatidylserine; pPE, plasmenylethanolamine; CAR, carnitine. **b**,**c**, Total accumulation of LA and AA (**b**) and lysophospholipids (**c**) in lumbar DRG and spinal cords of mice on either diet ($n=6$ per group). $^{****}P<0.0001$ (**b**), $^{***}P=0.0002$ (**c**, lysophosphatidylethanolamine), $^{**}P=0.0044$ (**c**, lysophosphatidylcholine). **d**, *Pla2* isozyme transcript expression in lumbar DRG ($n=6$ mice per group). **e**, Schematic detailing changes to a fluorogenic BODIPY substrate following *sn*-2 bond cleavage by PLA2 enzymes. FRET, fluorescence resonance energy transfer. **f**, PLA2 activity in DRG homogenates in response to pretreatment with vehicle (dimethyl sulfoxide (DMSO)) or the PLA2G7-selective inhibitor darapladib ($n=3$ biologically independent mouse samples per group). $^{****}P<0.0001$ for H6D, 0 μM darapladib versus L6D, 0 μM darapladib; $^{\#\#\#\#}P<0.0001$ for L6D, 1.5 μM darapladib versus L6D, 0 μM darapladib; $^{\#\#\#}P=0.0005$ for L6D, 0.15 μM darapladib versus L6D, 0 μM darapladib; $^{\$\$\$\$}P<0.0001$ for H6D, 1.5 and 0.5 μM darapladib versus H6D, 0 μM darapladib; $^{\$\$}P=0.0059$ H6D, 0.015 μM darapladib versus H6D, 0 μM darapladib. Max, maximum; min, minimum; RFU, relative fluorescence units. **g**, Acute effects (30 min) of intraplantarly (i.pl.) injected darapladib (DARA) on heat- and mechanical-evoked nociception. Bold lines represent mean ± s.e.m. determined from individual animal responses (faint lines) before and after treatment (L6D, $n=9$; H6D, $n=8$). $^{***}P=0.0003$ (left), $^{****}P<0.0001$ (right). BL, baseline. **h**, Withdrawal responses to heat and mechanical stimulation following daily i.t. (once a day (q.d.) × 3 d) injection with either scrambled or *Pla2g7*-directed siRNA (L6D, scrambled, $n=9$; H6D, scrambled, $n=10$; L6D, *Pla2g7*, $n=9$; H6D, *Pla2g7*, $n=9$). $^{****}P<0.0001$ (scrambled). All data are mean ± s.e.m. Error bars may be within the size of the symbol. Statistical tests used were two-way ANOVA (**b**,**c**), mixed-effects ANOVA (**g**) and one-way ANOVA (**f**,**h**), all with Sidak's post hoc test.

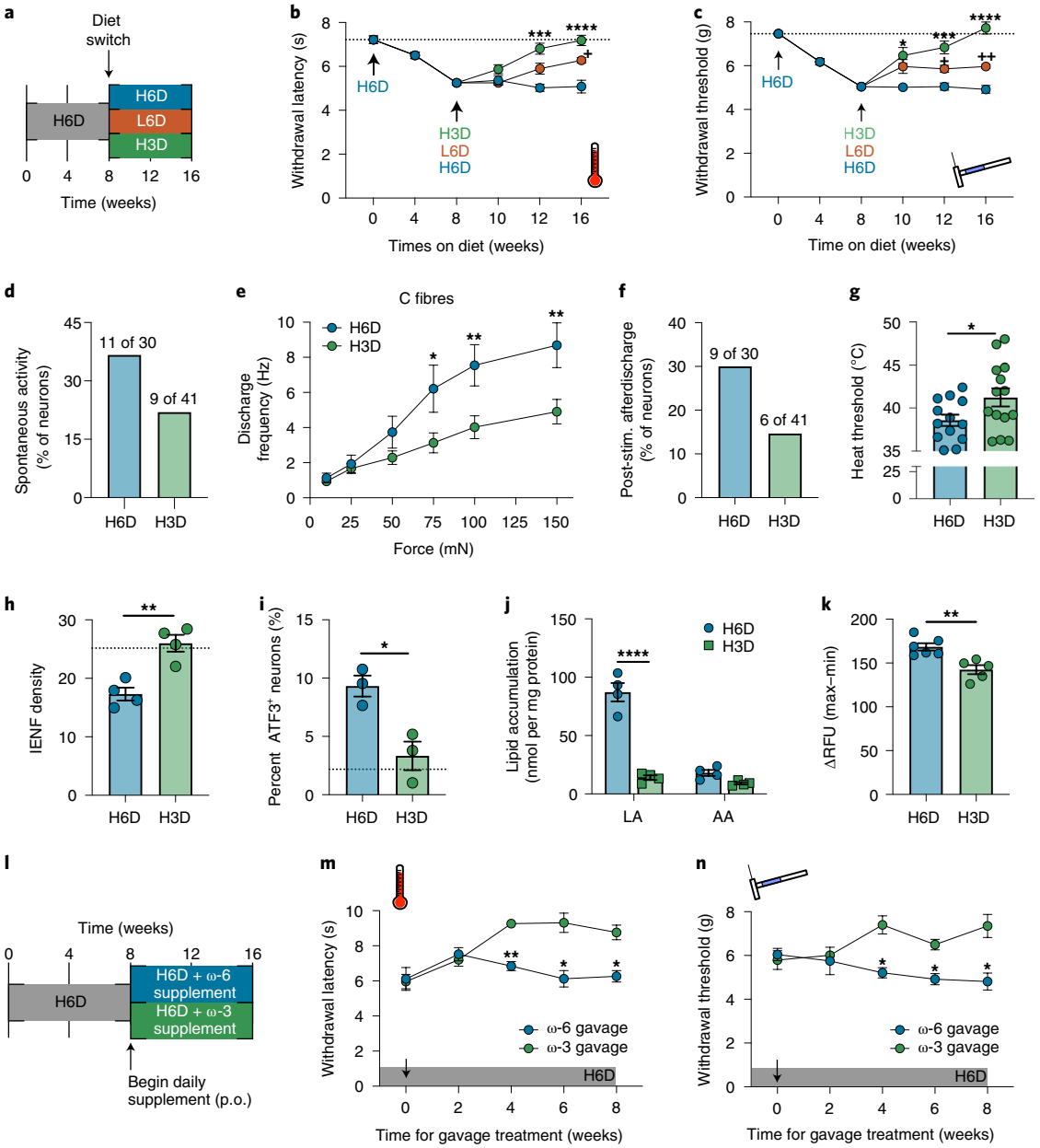

Fig. 3 | An ω-3 fatty acid–enriched diet rescues the H6D-induced neuropathy-like phenotype. a, Schematic of the diet-reversal paradigm, showing mice after 8 weeks on the H6D either continuing on the H6D, receiving the L6D or receiving a high 7.3% ω-3 PUFA diet (H3D) for 8 additional weeks. **b**,**c**, Effects of the H3D reversal on H6D-induced heat (**b**) and mechanical (**c**) hypersensitivities (H6D, $n=11$; L6D, $n=12$; H3D, $n=12$). ****$P<0.0001$ for H3D, 16 weeks versus H6D, 16 weeks (**b**,**c**); ***$P=0.0002$ for H3D, 12 weeks versus H6D, 12 weeks (**b**); ***$P=0.0008$ for H3D, 12 weeks versus H6D, 12 weeks (**c**); *$P=0.0363$ for H3D, 10 weeks versus H6D, 10 weeks (**c**); $^{++}P=0.0014$ for L6D, 16 weeks versus H6D, 16 weeks (**c**); $^{+}P=0.0352$ for L6D, 16 weeks versus H6D, 16 weeks (**b**); $^{+}P=0.0285$ for L6D, 12 weeks versus H6D, 12 weeks (**c**). **d**, Percentage of spontaneously active fibres (H6D, $n=30$; H3D, $n=41$). **e**, Discharge frequencies of mechanical-responsive C fibres during stimulation (H6D, $n=11$; H3D, $n=12$). **$P=0.0072$ (H3D, 150 mN), **$P=0.0094$ (H3D, 100 mN), *$P=0.0285$ (H3D, 75 mN). **f**, Percentage of fibres exhibiting post-stimulus (post-stim.) afterdischarge following mechanical force application (H6D, $n=30$; H3D, $n=41$). **g**, Heat thresholds of heat-responsive fibres (H6D, $n=13$; H3D, $n=14$). *$P=0.0466$. **h**, IENF densities (H6D, $n=4$; H3D, $n=4$). **$P=0.003$. **i**, Percentage of ATF3^{+} neurons in lumbar DRG (H6D, $n=3$; H3D, $n=3$). *$P=0.0169$. Dotted lines (**h**,**i**) reflect historical mean IENF density and percent ATF3^{+} neurons, respectively, from C57BL6/J mice on the L6D. **j**, Total accumulation of LA and AA in mouse lumbar DRG (H6D, $n=4$; H3D, $n=4$). ****$P<0.0001$ (LA). **k**, PLA2 activity in DRG homogenates (H6D, $n=6$; H3D, $n=5$). **$P=0.0043$. **l**, Schematic of the 16-week H6D with supplementation paradigm, showing that, after 8 weeks on the H6D, mice begin to receive either an additional ω-6 or ω-3 fatty acid supplement daily via gavage in addition to the H6D. p.o., per os. **m**,**n**, Effects of ω-6 and ω-3 fatty acid supplements on H6D-induced heat (**m**) and mechanical (**n**) hypersensitivities (ω-6, $n=4$; ω-3, $n=4$). **$P=0.0023$ (**m**, 4 weeks), *$P=0.0243$ (**m**, 6 weeks), *$P=0.0194$ (**m**, 8 weeks), *$P=0.0333$ (**n**, 4 weeks), *$P=0.0205$ (**n**, 6 weeks), *$P=0.0492$ (**n**, 8 weeks). All data are mean ± s.e.m. Statistical tests used were mixed-effects ANOVA with Geisser–Greenhouse's correction and Tukey's post hoc test (**b**,**c**), two-way ANOVA with Sidak's post hoc test (**e**,**j**,**m**,**n**) and unpaired two-tailed Student's *t*-test with Welch's correction (**g**–**k**).

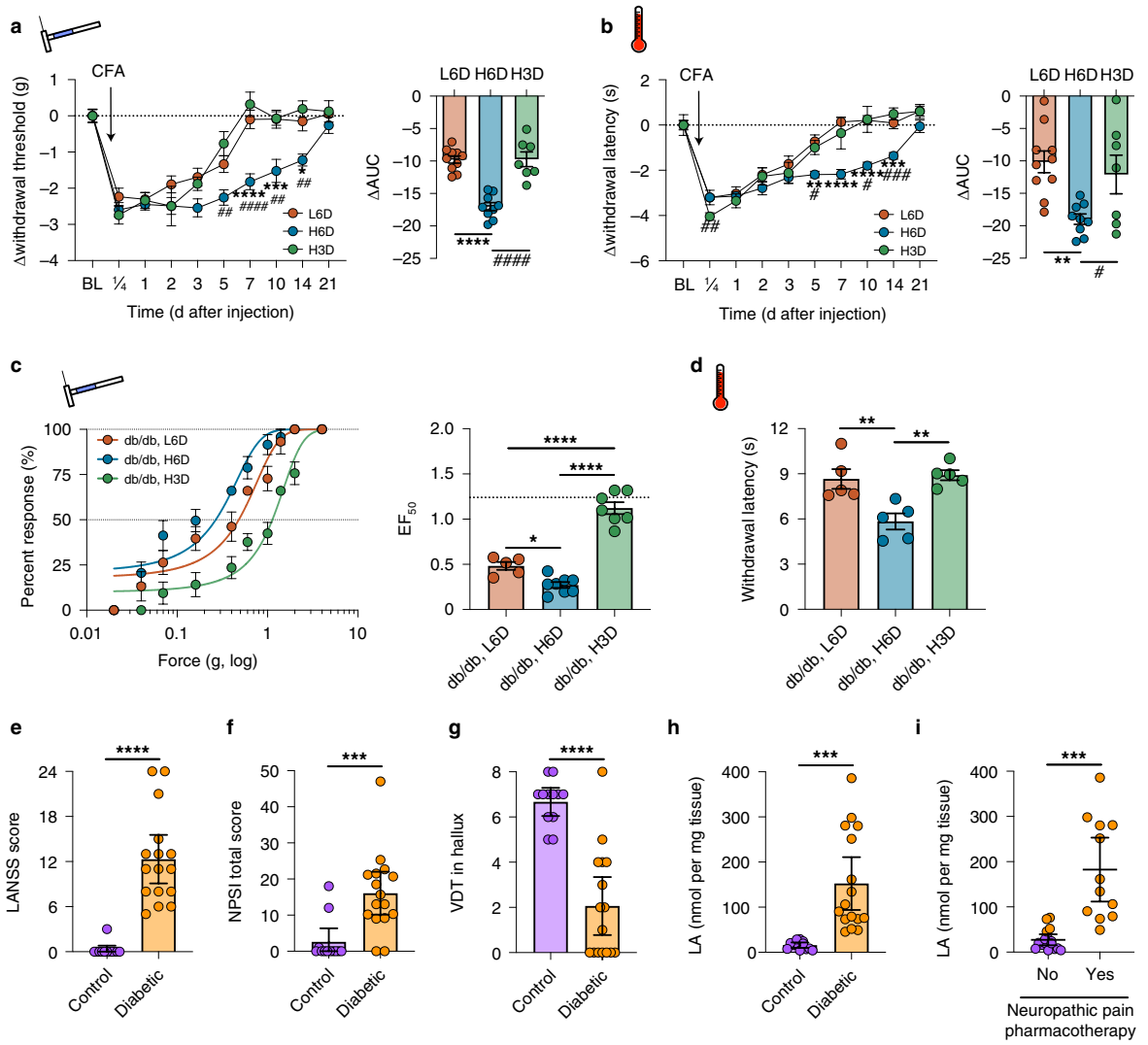

Fig. 4 | Diet-specific modulation of nociceptive behaviours associated with inflammatory and neuropathic pain. a,**b**, Time course of L6D-, H6D- and H3D-specific changes to withdrawal responses from mechanical (**a**) and heat (**b**) stimulation following administration of CFA. The change from baseline was calculated for each mouse as mean pre-CFA baselines differing across groups. Right (**a**,**b**), areas under the curve (AUC) (L6D, $n=10$; H6D, $n=9$; H3D, $n=7$). Time courses (comparisons to the H6D): $^{\#\#\#\#}P<0.0001$ for H3D, 7 d (**a**); $^{\#\#}P=0.0013$ for H3D, 5 d (**a**); $^{\#\#}P=0.0021$ for H3D, 10 d (**a**); $^{\#\#}P=0.0032$ for H3D, 14 d (**a**); $^{****}P<0.0001$ for L6D, 7 d (**a**); $^{***}P=0.0005$ for L6D, 10 d (**a**); $^{*}P=0.0334$ for L6D, 14 d (**a**); $^{\#\#\#}P=0.0003$ for H3D, 14 d (**b**); $^{\#}P=0.0174$ for H3D, 5 d (**b**); $^{\#}P=0.0266$ for H3D, 10 d (**b**); $^{****}P<0.0001$ for L6D, 7 or 10 d (**b**); $^{***}P=0.0013$ for L6D, 14 d (**b**); $^{**}P=0.0021$ for L6D, 15 d (**b**). AUC (comparisons to the H6D): $^{\#\#\#\#}P<0.0001$ for H3D (**a**), $^{****}P<0.0001$ for L6D (**a**), $^{\#}P=0.0472$ for H3D (**b**), $^{**}P=0.0045$ for L6D (**b**). **c**, Mechanical force–response curves (left) with EF_{50} values (right) determined with nonlinear regression for 12-week-old db/db mice fed either the L6D, the H6D or the H3D for 6 weeks (L6D, $n=5$; H6D, $n=8$; H3D, $n=7$). The dotted line (EF_{50} plot) reflects the historical mean EF_{50} value for C57BL6/J mice on the L6D. $^{****}P<0.0001$ for L6D and H6D versus H3D, $^{*}P=0.0244$ for L6D versus H6D. **d**, Paw-withdrawal latencies in response to radiant heat stimulation. $^{**}P=0.0064$ for L6D versus H6D, $^{**}P=0.0035$ for H3D versus H6D. **e**–**g**, Scatterplots of LANSS Pain Scale scores (**e**), NPSI total scores (**f**) and hallux vibration-detection thresholds (VDT) (**g**, arbitrary units) for controls (purple) and participants with diabetic neuropathy (orange) (control, $n=12$; diabetic, $n=16$). $^{****}P<0.0001$ (**e**,**g**), $^{***}P=0.0005$ (**f**). **h**,**i**, Total LA content in skin biopsies from the lateral malleolus. Participants are grouped based on diagnosis (**h**) or whether they were actively prescribed a neuropathic pain pharmacotherapy regimen (**i**). $^{***}P=0.0002$ (**h**), $^{***}P=0.0005$ (**i**). Data are mean ± s.e.m. (**a**–**d**) or mean ± 95% confidence intervals (**e**–**i**). Error bars for some data points are within the size of the symbol. Statistical tests used were two-way ANOVA with Geisser–Greenhouse's correction and Tukey's post hoc test (**a** (time), **b** (time)), one-way ANOVA with Tukey's post hoc test (**a** (AUC), **b** (AUC), **c**,**d**), unpaired two-tailed Mann–Whitney test (**e**–**g**) and unpaired two-tailed Student's *t*-test (**h**,**i**).

levels and decreasing ω-6 fatty acid levels are required to reverse the H6D-induced phenotype.

Clinically, the development of one pain condition markedly increases the risk of developing additional pain comorbidities[43]. Thus, we next questioned whether the H6D would exacerbate and/or prolong nociceptive hypersensitivity under conditions of inflammatory or neuropathic injury. To model persistent inflammatory pain[44], L6D-, H6D- and H3D-fed mice were injected with complete Freund's adjuvant (CFA). The H6D prolonged CFA-induced heat and mechanical hypersensitivities threefold compared to those in L6D- and H3D-fed mice (Fig. 4a,b). We again used db/db mice to model type 2 diabetes–associated peripheral neuropathy[45,46]. Diabetic mice on the H6D for only 6 weeks developed a greater mechanical allodynia compared to db/db mice on the L6D, whereas those on the H3D did not exhibit mechanical allodynia but rather mechanical responses commensurate with those

from historical C57BL6/J control mice on normal chow (Fig. 4c). Interestingly, db/db mice given either the L6D or the H3D exhibited normal responses to noxious heat stimulation, contrasting the hypersensitivity induced by the H6D (Fig. 4d). Together, these data suggest that an H6D risks prolonged and/or exacerbated pain when coupled with persistent inflammation or neuropathic injury but also can be ameliorated with an H3D supplement.

These findings could have far-reaching clinical importance. Considering the clinical link between dietary LA intake and diabetes[47], along with our findings in diabetic mice, we next tested for associations between skin ω-6 fatty acid levels and pain symptoms reported by participants with diabetes and painful neuropathy (Supplementary Table 2). Compared to age-matched non-diabetic controls, participants with diabetic neuropathy reported more neuropathic pain-related symptoms, based on scores derived from the Leeds assessment of neuropathic symptoms and signs (LANSS) Pain Scale[48] and the Neuropathic Pain Symptom Inventory (NPSI) questionnaire[49], and exhibited diminished vibration-detection thresholds of the halluces (Fig. 4e–g). Moreover, total LA content was substantially elevated in ankle skin biopsies from participants with diabetes (Fig. 4h and Extended Data Fig. 8a). Despite the small sample size ($n=28$ total participants), robust correlations were observed between skin LA levels and all three clinical indices (Extended Data Fig. 8b–d). We also grouped participants based on active prescriptions for medications commonly used to manage neuropathic pain (for example, gabapentinoids, selective serotonin-reuptake inhibitors, serotonin–noradrenaline-reuptake inhibitors). Remarkably, 75% (12 of 16) of participants with diabetes and elevated LA levels required neuropathic pain pharmacotherapy (Fig. 4i). The four participants with diabetes not receiving treatment showed LA levels below 100 nmol per mg tissue. Four participants with diabetes and prescribed neuropathic pharmacotherapy also had low skin LA levels. Interestingly however, they were either on a starting dose of the medication, rated pain below 5 (scale of 0–10) or reported >90% pain relief (Supplementary Table 2). These data suggest that patients with low skin LA levels may be best managed conservatively with either symptomatic analgesics or low-dose neuropathic pharmacotherapy, while patients with LA levels >100 nmol per mg require more robust intervention with neuropathic pharmacotherapy. We believe that these data warrant continued investigation of peripheral fatty acid and metabolite levels as potential pain biomarkers. Such biomarkers could provide clinicians with reliable objective endpoints to guide diagnoses as well as decision making on treatment regimens, including therapeutic diets.

In summary, we demonstrated that an ω-6 PUFA-enriched diet loads DRG and skin with LA and AA within 8 weeks, leading to elevated PLA2-mediated lipid release, the onset of peripheral nerve damage and the development of nociceptive hypersensitivity. Our findings support the inclusion of pain disorders with other prominent diseases that necessitate medical oversight of patients' diets. We also propose diet as a pain-risk factor, based on observations that elevated ω-6 PUFA levels exacerbate nociceptive hypersensitivities in preclinical models of inflammatory and neuropathic pain, as well as robust clinical associations determined between skin LA content and multiple pain indices in diabetic neuropathy. These are consistent with patients with a high body mass index being increasingly susceptible to chronic pain conditions[50,51]. We further show that darapladib, a PLA2G7-selective inhibitor under clinical investigation for non-pain conditions[52,53], attenuates H6D-induced hypersensitivity, while dietary replacement with ω-3 PUFAs completely reverts the phenotype. While these both may provide new approaches for management of chronic pain disorders, the role of PLA2G7 is particularly intriguing, considering the recent association of a loss-of-function polymorphism with reduced migraine risk[54] as well as the identification of several expression quantitative trait loci in human DRG tissue[55]. And, while it is unknown whether a PLA2G7 inhibitor would diminish concomitant diet therapy, for example, future exploration is still needed, given the lack for effective analgesics for so many prevalent pain conditions.

Methods

Animals. All animal experiments conformed to the Guidelines for the Use of Animals in Research as put forward by the International Association for the Study of Pain and to protocols approved by the University of Texas Health Science Center at San Antonio (UTHSCSA) Animal Care and Use Committee. Mouse experiments were initiated at 8–10 weeks of age in both male and female C57BL/6J mice (000664, Jackson Laboratory). Male BKS.Cg-*Dock7*^{m} +/+ *Lepr*^{db}/J (db/db[56], 000642, Jackson Laboratory) mice 16 weeks of age were used as positive controls to model a diabetic neuropathy phenotype. Mice were housed in groups of four to five, were maintained on a 12-h light–dark cycle with ambient temperatures between 20 and 22 °C and had free access to food and water.

Diets. Randomised groups of mice were fed isocaloric diets containing 10% g per kg total fat with an energy density of 22.9% kcal per kg for at least 8 weeks to maintain equivalency of nutrient and calorie intake. The L6D, H6D and H3D were formulated by Dyets based on the AIN-93G diet[57] and modified to control the amount of ω-6 or ω-3 PUFAs (Supplementary Table 1). As described previously[27], the H6D consisted of 11.8% kcal per kg ω-6 PUFAs, 1.0% kcal per kg ω-3 PUFAs, 2.2% kcal per kg MUFAs and 7.9% kcal per kg SFA (Dyets, 181189), and the L6D consisted of 0.4% kcal per kg ω-6 PUFAs, 1.0% kcal per kg ω-3 PUFAs, 1.2% kcal per kg MUFAs and 20.3% kcal per kg SFA (Dyets, 180784). The H3D consisted of 0.9% kcal per kg ω-6 PUFAs, 8.6% kcal per kg ω-3 PUFAs, 6.0% kcal per kg MUFAs and 7.0% kcal per kg SFA (Dyets, 104593). For rescue experiments, mice were placed on the H6D for 8 weeks and then switched to either the H6D or the H3D for at least another 8 weeks. All diets were stored at −20 °C and used for no longer than 6 months. Food was replaced weekly. Animals and food were weighed weekly to monitor changes in body weight and food consumption. Weekly food intake (per cage of five mice) was calculated by the change in food weight measured at the beginning and end of each week. Normal chow consisting of 2.6% kcal per kg ω-6 PUFAs, 0.3% kcal per kg ω-3 PUFAs, 1.3% kcal per kg MUFAs and 0.8% kcal per kg SFA (Teklad LM-485, Envigo) was given to control and db/db mice for metabolic comparison.

For the oral gavage experiment, following 8 weeks on the H6D, mice received orally 200 µl (q.d., p.o.) of either high LA safflower oil (BodyBio, SP125, ~424 mg LA daily) or an over-the-counter fish oil (Carlson, the Very Finest Fish Oil, Norwegian, ~64 mg ω-3 fatty acid daily, 32 mg EPA, 20 mg DHA) on Mondays through Fridays in addition to the H6D ad libitum for 8 weeks. A recovery period was allowed on Saturdays and Sundays to not overly stress the mice from gavage volume.

Behavioural testing. All experiments were performed by blinded observers, and the assay order was randomised on each testing day.

Mechanical stimulation assays. Paw-withdrawal thresholds in response to noxious mechanical stimulation were evaluated using the Ugo Basile Dynamic Plantar Aesthesiometer equipped with an 0.8-mm rigid von Frey filament as previously described[58]. Briefly, animals were randomised into plastic observation boxes on an acrylic grid platform and acclimated for 60 min. The aesthesiometer was positioned under the mouse to stimulate the mid-plantar area of the hindpaw with a force ramp up to 15*g* over a 7-s period. The force at which withdrawal occurred was recorded. All animals were tested a minimum of three times, and the average was used for statistical analysis. To more thoroughly characterise mechanical hypersensitivity, a range of von Frey fibres from 0.008 to 4*g* (11 fibres) were used as described previously[59]. Briefly, mice were acclimated in observation boxes on a wire-mesh floor for 60 min. Von Frey fibres contacted the mid-plantar surface of the hindpaw until slight buckling of the filament was observed and then were held for 2 s. Each fibre was probed five times per mouse with at least 30 s between applications. Withdrawal of the paw was noted as a positive response, and no movement was considered a negative response. Values were recorded as percent response for each fibre. Force–response curves were generated using nonlinear least-squares regression of the mean and used to calculate the EF_{50} (ref. [60]).

Brush test. Dynamic tactile response was assessed using a cotton swab brushed quickly across the plantar surface of the hindpaw as described previously[61]. Animals were acclimated for 30–60 min in boxes above mesh-grid flooring. The 'puffed out' cotton swab was used to brush the length of the ventral hindpaw in a continuous motion. Positive responses were defined as withdrawal or rapid shaking of the paw. Each animal was tested five times on each paw with a minimum of 30 s between tests.

Heat-stimulation assay. Paw-withdrawal latency (s) in response to heat stimulation was assessed using the radiant heat test[62]. Animals were acclimated in plastic observation boxes for 30–60 min before testing. The mid-plantar surface of the mouse hindpaw was exposed to a radiant heat source through a glass floor until paw withdrawal. The intensity of the heat source was adjusted to produce

a standard baseline of ~8 s in naive wild-type mice, with a maximum cutoff of 20 s. All animals were tested a minimum of three times with at least 60 s between recordings, and the average of all recordings was used for statistical analysis. Mechanical thresholds were determined from the same animals on the same days.

Cold-stimulation assay. Response to cold stimulus was measured according to an adaptation of a previously described protocol[63]. Mice were placed in plastic observation boxes on top of a 3/16-inch tempered glass flooring and allowed to acclimate for at least 30 min. A 10-ml syringe was sectioned above the Leur lock and tightly packed with finely crushed dry ice. The syringe was pressed firmly on the bottom of the tempered glass directly below the hindpaw while measuring paw-withdrawal latency (s) with a stop watch. Thickness of tempered glass and syringe size were selected to establish baseline measurements of ~8 s. Each animal was tested three times on each paw with a minimum of 1 min between tests.

Complete Freund's adjuvant pain model. CFA (Sigma) was diluted 1:1 with saline and injected intraplantarly into the right hindpaw of mice using a 30G insulin syringe filled to 20 µl. Thermal and mechanical readings were taken before injection and then at 0.25, 1, 2, 3, 5, 7, 10, 14 and 21 d after injection. Animals were followed until they returned to the original baseline thresholds. As pre-CFA baselines were different between diet cohorts, data were normalised as the change from the baseline withdrawal response.

Blood sampling. HbA1c and fasting blood glucose levels were measured in mice after 8 weeks on either the H6D, the L6D or the H3D. Whole blood was collected from the submandibular branch of the jugular vein into EDTA-coated Microvette CB 300 collection tubes (Kent Scientific). HbA1c levels were determined using a mouse whole-blood assay kit according to the manufacturer's instructions (83010, Crystal Chem). Briefly, whole blood was mixed with lysis buffer for 10 min and then mixed with protease buffers and incubated at 37 °C for 5 min. Absorbance was then measured at 700 nm on a VersaMax microplate reader (SoftMax Pro 7.1, Molecular Devices). To measure fasting blood glucose levels, mice first were fasted for 5 h to optimise the physiological context[64,65]. Next, a single drop of blood was collected from the submandibular branch of the jugular vein on a blood glucose test strip and analysed with the AlphaTRAK2 Blood Glucose Monitoring System. Blood from wild-type and db/db mice on normal chow served as negative and positive controls, respectively.

Shotgun lipidomics. DRG and spinal cord tissues were homogenised in 0.5 ml 10× diluted PBS in 2.0-ml cryogenic vials (Corning) by using the Precellys Evolution homogeniser (Bertin). Protein assays on homogenates were performed by using a BCA protein assay kit (Thermo Scientific) with BSA as the standard. The rest of the homogenate was accurately transferred into a disposable glass culture test tube, and a mixture of lipid internal standards was added before lipid extraction for quantification of all reported lipid species. Lipid extraction was performed by using a modified Bligh and Dyer procedure as described previously[66]. Individual lipid extracts were resuspended in a volume of 400 µl chloroform–methanol (1:1, vol/vol) per mg protein and flushed with nitrogen, capped and stored at −20 °C for lipid analysis. For shotgun lipidomics, lipid extracts were further diluted to a final concentration of ~500 fmol µl^{-1}, and mass spectrometric analysis was performed on a QQQ mass spectrometer (Thermo TSQ Quantiva) equipped with an automated nanospray device (TriVersa NanoMate, Advion Biosciences) as previously described[67]. Identification and quantification of lipid molecular species were performed using an automated software programme (Xcalibur)[68,69]. Data were normalised to protein levels (per mg). All membrane-bound lipids (defined as lipids attached to membrane-anchoring headgroups) were then grouped together, and total concentrations of ω-6 fatty acids, LA (18:2) and AA (20:4), were determined between L6D and H6D and used for statistical analysis.

Quantification of total tissue lipid levels. The lipid extraction protocol was adapted from the Bligh–Dyer method[70]. Briefly, frozen tissue samples were weighed and then sectioned on a cryostat at 16 µm and collected into cold-acclimated glass test tubes. Each tube was then placed on ice, received 2 ml extraction buffer (50% methanol, 25% chloroform, 20% ddH_2O, 0.02% butylated hydroxytoluene), was spiked with an internal standard (5 µl ml^{-1} LA-d_4, 1 µl ml^{-1} AA-d_8, 1 µl ml^{-1} EPA-d_5, 1 µl ml^{-1} DHA-d_5 and 5 µg ml^{-1} α-linolenic acid-d_{16}) and was vortexed for 30 s every 5 min for 15 min. Samples were centrifuged at 5,000*g* and 4 °C for 10 min, and the bottom organic phase was collected in a separate glass tube. The aqueous phase was re-extracted with 1 ml extraction buffer, and, following collection of the second bottom phase, samples were dried down under a steady stream of nitrogen. To analyse total lipid pools, samples next underwent base-catalysed saponification as described previously[71,72]. Briefly, dried samples were resuspended with 850 µl methanol–chloroform solution (8:1) and 150 µl 40% potassium hydroxide solution, placed under nitrogen and then heated to 37 °C for 60 min. Following this, samples received 700 µl 0.05 M phosphate buffer and 300 µl 1 M HCl (pH < 5) and then were extracted twice with 2 ml hexane. Both upper phases were combined and then dried down under nitrogen. Samples were stored at −80 °C until processing with LC–MS/MS.

Dried samples were reconstituted with 150 µl ethanol and transferred to 1-ml autosampler vials for LC–MS/MS. A Waters Acquity UPLC system was used to perform reversed-phase separation of free fatty acids. A Thermo Electron BDS Hypersil C18 column (50-mm × 2.1-mm i.d.) with a particle size of 5 µm was held at 45 °C. Solvent A was 5 mM ammonium acetate in water, and solvent B was acetonitrile with 10% 2-propanol and 0.2% acetic acid. All solvents were Fisher Scientific Optima LC–MS grade. The gradient was set up as follows: 0 min (40% A:60% B), 4 min (5% A:95% B), 4.5 min (5% A:95% B), 4.6 min (40% A:60% B), 6.5 min (40% A:60% B). The autosampler was held at 5 °C. The injection volume was 5 µl, and the flow rate was constant at 0.5 ml min^{-1}. A TQD tandem quadrupole mass spectrometer (Waters) was used to determine free fatty acid concentrations. An ESI source in negative ion mode was used with the capillary voltage set to 1.5 kV. The source temperature was set at 150 °C with a desolvation temperature of 400 °C. Argon was used as the collision gas for CID at 0.10 ml min^{-1}, and nitrogen was used for the cone gas flow at 121 h^{-1} and the desolvation gas flow at 600 l h^{-1}. Multi-reaction monitoring channels were used for both LA and AA, but, as LA does not produce detectable fragment ions, the channel used the parent ion mass of 279.2 Da for the fragment ion as well. This excludes species of the same mass that do produce fragment ions. AA multi-reaction monitoring transitions were 303.2 → 205 (*m*/*z*) and 303.2 → 259 (*m*/*z*). The collision energy for LA and AA was 10 eV. Waters software TargetLynx was used to perform channel integration and smoothing. Analytical standards of LA and AA (Cayman Chemical) were used to establish calibration curves. The calibration ranged from 10 ppm to 10 ppb for each standard in ethanol.

Single-fibre recordings of glabrous skin–tibial nerve preparations. To provide a neurophysiological correlate to H6D-induced behaviours, we used ex vivo glabrous skin–tibial and sural nerve preparations as described previously[73–77]. Tibial and sural nerves were selected based on anatomical distribution of terminal nerve endings within the glabrous skin of the mouse hindpaw[78], using the same region tested for evoked behavioural assays described above. Mice were briefly anaesthetised with isoflurane and then killed via cervical dislocation. The right leg was shaved followed by careful dissection of the skin–nerve preparation, which included the glabrous skin and attached tibial and sural nerves. The preparation was transferred to the organ bath chamber of a 3D-printed stage (courtesy of P. Reeh, University of Erlangen–Nuremberg) with oxygenated standard interstitial fluid (SIF, pH 7.4) consisting of 123 mM NaCl, 3.5 mM KCl, 2.0 mM $CaCl_2$, 0.7 mM $MgSO_4$, 1.7 mM NaH_2PO_4, 9.5 mM $NaC_6H_{11}O_7$, 5.5 mM glucose, 7.5 mM sucrose, 10 mM HEPES and perfusing at 32 ± 0.7 °C (Eco Silver, LAUDA-Brinkmann) at a flow rate of 15–16 ml min^{-1} (Masterflex L/S, Cole-Parmer). The skin was positioned corium-side up and pinned down with insect needles to a silicon rubber base (Sylgard 184, Dow Corning) in the organ chamber. The nerve was threaded through a 1-mm hole into the adjacent recording chamber and placed on top of a mirror plate. Low-viscosity mineral oil (M5904, Sigma) was applied onto the nerve on the mirror plate during teasing and recording to electrically isolate it from the rest of the perfusion chamber. Using a stereomicroscope (SMZ745T, Nikon) positioned over the recording chamber, the nerve was desheathed, and single filaments were carefully teased apart for recording. Teased filaments were wrapped around a 0.25-mm silver wire electrode (AGW1010, World Precision Instruments) to record activity. Both the reference (grounded extracellular milieu) and recording (nerve) electrodes in the recording chamber fed into a low-noise headstage probe (DAM80p, World Precision Instruments), which relayed the signal to a DAM80 differential amplifier (World Precision Instruments). Incoming signals were amplified 1,000-fold and bandpass filtered between 300 and 1,000 Hz. Amplified signals were filtered through a Hum Bug 50/60 Hz Noise Eliminator (Quest Scientific) and then passed to a TBS1000B digital oscilloscope (Tektronix), a model 330 audio monitor (A-M Systems) and a Micro1401-3 digital data-acquisition system (Cambridge Electronic Design). Data were recorded with Spike2 (Cambridge Electronic Design).

Sensory profiling of teased fibres. Receptive fields (RF) were initially identified based on mechanical responsiveness to a blunt glass rod. Upon positive identification of an RF, the following steps were used to characterise the sensory profile of the teased fibre: (1) spontaneous activity (the presence of spontaneous activity was assessed for the first 2 min of recording), (2) mechanical stimulation (a precision force-controlled mechanical stimulator (series 300C-I Dual Mode Servo System, Aurora Scientific) was used to evaluate fibre mechanosensitivity. The mechanical cylinder (0.7-mm tip diameter) was positioned over the RF of interest, followed by computer-controlled application of square force stimuli (force range of 5–200 mN with a 10-s duration). To prevent sensitisation or desensitisation of the recorded fibre, 60-s intervals were given between force applications), (3) heat stimulation (a Peltier-based thermal stimulus delivery system (CS1, Cool Solutions) was used to assess fibre responsiveness to controlled heat application[79]. A custom-designed cylindrical ring (OnShape) that was 3D-printed on a Form 2 using Tough Resin (Formlabs) was used to isolate the RF of interest. Vacuum grease (Dow Corning) tightly sealed the ring in position. An insulated afferent tube connected to the Peltier device, an efferent tube and a thermocouple were then positioned within the ring. A dispensing pump (IPC24, Ismatec) drove the push–pull superfusion (60 µl s^{-1}) of SIF over the RF within the ring (Extended Data Fig. 2c). The SIF temperature increased from 30 °C to 52.0–60.5 °C during heat ramps (30 s). After 30 s of heating, Peltier stimulation was stopped, and temperature returned to

baseline within 90 s. Intervals of at least 5 min were given between heating to prevent sensitisation or desensitisation of the isolated RF), (4) conduction velocity (a 2.0-MΩ parylene-coated tungsten metal stimulating electrode (TM33B20, World Precision Instruments) was positioned within the RF of interest. A stimulus isolator (A365, World Precision Instruments) and pulse generator (A310, World Precision Instruments) were used to deliver electrical pulses to the RF. Upon electrical stimulation of the fibre, digital calipers were used to measure the conduction distance (in mm) between the RF and the recording electrode. Conduction velocity was calculated by dividing this distance by the latency of the firing fibre from the stimulating artefact and was represented in units of $m\,s^{-1}$.

Spike detection and analysis. Recordings were analysed with offline template matching in Spike2 version 8.14 (Cambridge Electronic Design). Settings for spike template matching required a minimum of 70% of sampling points within a template and a maximum change in amplitude of 25%. Waveform data were interpolated linearly. The high-pass-filter time constant was set to 6.4 ms. Triggers were set at least three times the baseline noise level. Conduction velocity, calculated by dividing the conduction distance over the spike electrical latency, was used to classify fibre type according to the following cutoffs: C fibres $<0.8\,m\,s^{-1}$, AM fibres $>1.2\,m\,s^{-1}$ (ref. [80]). Spontaneously active fibres were defined with a minimum unprovoked discharge frequency of 0.1 Hz[81]. Mechanical discharge frequencies were determined for each force application as the number of firings within the 10-s ramp period. Post-stimulus afterdischarge was identified as persistent activity occurring after completion of any force ramp. For heat responses, total afferent activity was used instead of discharge frequency, as recordings often included individual units with variable amplitudes that could not always be discriminated[74]. Heat threshold temperatures were identified as the temperature that initiated the first afferent activity during a heat ramp. Post-stimulation activity was calculated as the number of action potentials during the time period, defined as the point when the recovering temperature reached a fibre's heat threshold through to baseline.

Immunohistochemistry and imaging. L3–L5 DRG and 3-mm biopsies of glabrous hindpaw skin were immediately dissected after killing. Tissues were fixed by immersion in 4% paraformaldehyde in 0.1 M phosphate buffer for 2 h. Tissue samples were washed for 15 min three times with phosphate buffer, immersed in 10% sucrose at 4 °C overnight, transferred to 30% sucrose at 4 °C overnight and then stored at −20 °C. For cryosectioning, tissues were thawed and placed in OCT (Tissue-Tek) before freezing on dry ice. Sections of DRG (14 µm) and paw tissue (20 µm) were cut with a cryostat (Microm HM550, Thermo Fisher Scientific) and thaw mounted onto Superfrost Plus slides (Fisherbrand). Slides were air dried at room temperature (RT) and stored at −20 °C. Staining was performed using the MAXpack Immunostaining Media kit (Active Motif). Tissue sections were blocked with MAXblock Blocking Medium for 1 h at RT, followed by incubation with primary antibodies diluted in MAXbind Staining Medium at 4 °C overnight. Primary antibodies included anti-PGP9.5 (1:1,000, AB1761-I, Millipore), anti-ATF3 (1:400, ab207434, Abcam), anti-NeuN (1:500, ABN91, Millipore), anti-NFH (1:5,000, 822601, BioLegend), anti-TRPV1 (1:700, GP14100, Neuromics), anti-PLA2G7 (1:500, 15526-1-AP, ProteinTech) and anti-GFRA2 (1:500, AF429, R&D Systems). Isolectin GS-IB4 Alexa Fluor 488 conjugate (1:800 from stock, 121411, Thermo Fisher) was used during primary incubation as well. Sections were then washed for 10 min three times with MAXwash solution and incubated with secondary antibodies for 1 h at RT. The following secondary antibodies (Jackson ImmunoResearch) were used: Alexa Fluor 488 AffiniPure donkey anti-chicken IgY (IgG) (H+L), Alexa Fluor 488 AffiniPure donkey anti-rabbit IgG (H+L), Alexa Fluor 568 donkey anti-rabbit IgG (H+L), Alexa Fluor 647 AffiniPure donkey anti-guinea pig IgG (H+L), Rhodamine Red-X AffiniPure donkey anti-goat IgG (H+L), all at a dilution of 1:500 from stock. After washing for 10 min three times with MAXwash, DAPI ($0.02\,\mu g\,ml^{-1}$, Sigma, D9542) was applied for 10 min at RT, followed by two 10-min washes with MAXwash and then two 5-min washes with ddH_2O. Slides were air dried in the dark for 20 min and then were mounted with ProLong Diamond (Thermo Fisher Scientific) and no. 1.5 high-precision cover slips (Zeiss) for imaging.

Confocal microscopy. Images were obtained with a Nikon C1si laser scanning confocal microscope equipped with a 402-nm diode, a 488.1-nm solid state, a 561.4-nm diode-pumped solid state and 639-nm diode lasers. Objectives (Nikon) used included an ×10, 0.4-NA Plan Apo air, an ×20, 0.75-NA Plan Apo DIC air and an ×40, 0.95-NA collar-corrected Plan Apo air. Image-acquisition settings were a resolution of 1,024 × 1,024, a 12-bit image depth, a scan speed of 2.0 µs per pixel, a 30-µm confocal aperture (pinhole diameter) and sequential channel scan. *z* stacks were taken at optical steps of 0.3–0.6 µm (×20 and ×40 objectives). All images for each tissue type were taken at identical gain settings. Laser power, HV and offset were adjusted to maximise dynamic range while avoiding pixel saturation (EZ-C1 version 3.8, Nikon). Adjustments of brightness and contrast, look-up tables and *z*-stack reconstructions were performed in Fiji[82–85].

Intraepidermal nerve fibre–density quantification. To evaluate changes in epidermal innervation density, immunolabelled IENFs projected across the dermal–epidermal junction to the epidermis were counted in randomly selected fields of view from each section. The following exclusion criteria were used when counting IENFs: (1) fragments of nerve fibres in the epidermis that did not clearly cross the dermal–epidermal junction were not counted, and (2) fibres that approached but did not cross the dermal–epidermal junction, as determined by basal epidermal autofluorescence, were not counted[86,87]. To reduce bias, counting was conducted by two blinded observers on three to five nonconsecutive sections per animal with four animals per group. The averaged fibre count for each section was divided by the length of the dermal–epidermal junction to calculate the IENF density (IENFs per mm tissue). Mean IENF density ± s.e.m. for each group were used to determine statistical significance.

ATF3 quantification. To measure changes in the expression of the transcription factor ATF3 as a marker of neuronal injury[20], the number of $ATF3^+$ neurons in immunolabelled sections from L3–L5 DRG were counted. Images underwent thresholding before manual counting of stained nuclei. For each image, the percentage of ATF3-labelled neurons was calculated by dividing total $ATF3^+$ neurons by total $NeuN^+$ neurons and multiplying by 100. Using Fiji, quantifications were performed on three to five non-overlapping sections per mouse to determine individual means. Group mean ± s.e.m. were calculated using individual means from three to four mice per group.

PLA2 activity assay. DRG from H6D-, L6D- and H3D-fed animals were dissected, placed into cold lysis buffer (50 mM Tris-HCl, pH 8, 2 mM dithiothreitol, 1 mM $MgCl_2$, cOmplete Mini Protease Inhibitor) and incubated on ice for 15 min. DRG were homogenised using a 2-ml Dounce homogeniser, transferred to 1.5-ml tubes and centrifuged for 20 min at 15,000*g* and 4 °C. Supernatants were collected into new 2-ml tubes. Total protein concentration was determined using the Bio-Rad Bradford protein assay kit according to the manufacturer's instructions (Thermo Fisher Scientific, 23225). An adapted BODIPY (Invitrogen, A10072) assay was used for continuous monitoring of PLA2 activity from homogenates based on the manufacturer's instructions and a previous publication. Briefly, a 1 mM stock of Red/Green BODIPY PC-A2 was prepared in DMSO. To prepare the liposome mixture, equal volumes of 10 mM DOPC, 10 mM DOPG and 1 mM BODIPY dye were mixed in a microcentrifuge tube and slowly injected into assay buffer while rapidly stirring. DRG lysates were added to microplate wells at appropriate concentrations. A buffer-only well was use as a negative control, and bee venom (PLA2G3) was used as a positive control. The liposome mixture was then added at a dilution of 1:1 to the microplate wells. In PLA2 inhibitor experiments, the drug was incubated with the DRG lysate for 15 min before addition of the liposomal substrate. A FlexStation 3 with SoftMax Pro 4.3 (Molecular Devices) was set to 37 °C and used for kinetic recording of 520-nm and 570-nm emission for 30 min. Peak maximum minus minimum fluorescence signals for each wavelength (arbitrary units) were used for statistical analysis of each sample.

In vivo treatment. All drugs were prepared in coded syringes on the day of injection by an individual not performing behavioural testing to blind the experimenter. Animals were initially acclimated to observation boxes on top of thermal or mechanical platforms for a minimum of 30 min before collection of baseline recordings. After baselines, animals were administered vehicle or testing compound. Darapladib (Selleckchem, SB-480848) was dissolved in DMSO and Tween-20 and then diluted in PBS to 2% of each for final concentrations of 300 nM and 30 nM. Control animals received an equivalent volume of the darapladib vehicle.

Knockdown of *Pla2g7* was performed using Dharmacon SMARTpool siRNA against four separate *Pla2g7* target sequences. Control groups received non-targeting scrambled siRNA (Dharmacon). PLA2g7 or scrambled siRNA was injected i.t. (2 µg) for 3 consecutive days for a cumulative dose of 6 µg. Behaviour was tested 2 d after the final injection by blinded observers, followed by collection of DRG for protein and transcript quantification.

Quantitative PCR. L3–L5 DRG were collected and immediately frozen on dry ice and then stored at −80 °C. DRG tissue was homogenised as described previously[88] in 900 µl QIAzol lysis reagent (Qiagen) and placed on ice for 5 min. RNA was isolated according to the manufacturer's instructions (Qiagen, RNeasy Plus Universal Mini Kit, 73404). Briefly, 100 µl gDNA eliminator and 180 µl chloroform were added to each tube and shaken for 15 s. Tubes were centrifuged at 12,000*g* for 15 min, and the top aqueous phase was removed for further purification with ethanol and wash buffers and elution with RNase-free water (NanoDrop, Thermo). cDNA was then synthesised from 1 µg RNA using the SuperScript III First-Strand Synthesis kit (Invitrogen, 18080051). Amplification of target sequences was performed using TaqMan Fast Advanced Master Mix (Applied Biosystems, 4444557), according to the manufacturer's instructions, and selected primers for *Rn18s* (Mm03928990_g1, Thermo Fisher), *Pla2g3* (Mm00555594_m1, Thermo Fisher), *Pla2g6* (Mm00479527_m1, Thermo Fisher), *Pla2g7* (Mm00479105_m1, Thermo Fisher), *Pla2g12* (Mm01316982_m1, Thermo Fisher), *Pla2g15* (Mm00505425_m1, Thermo Fisher), *Anxa1* (Mm00440225_m1, Thermo Fisher), *Anxa2* (Mm01150673_m1, Thermo Fisher), *Anxa3* (Mm00442685_m1, Thermo Fisher), *Anxa5* (Mm01293059_m1, Thermo Fisher) and *Anxa6* (Mm00478966_m1, Thermo Fisher). qPCR was performed using the StepOnePlus Real-Time

PCR System (Applied Biosystems, 4376600). A no-template control was used as a negative control. Cycles of thresholds (Ct) were collected and normalised to those of the internal control *Rn18s*. ΔΔCt values normalised to those of the *Rn18s* reference were used for statistical analysis[89].

Western blot. Reinforced screw-cap microtubes (2 ml) prefilled with 2.8-mm ceramic beads (19-628, Omni International) were filled with 900 µl RIPA buffer (Thermo Fisher, 89900) with cOmplete Mini Protease Inhibitors (Roche, 11836145001). Thawed DRG tissue samples were then transferred to bead tubes and placed on ice. The processing chamber of a Bead Ruptor 24 (Omni International, 19-040E) was precooled to 0 °C with an attached BR-Cryo Cooling Unit (Omni International, 19-8005). Samples were placed in the tube carriage, homogenised for 30 s at 7.10 m s^{-1} and then placed on ice for 5 min. Samples were transferred to fresh tubes and centrifuged for 3 min at 8,000*g* and 4 °C. Supernatants were collected and stored at −80 °C until use. After total protein determination, supernatants were prepared for SDS–PAGE on 4–12% gradient Bis-Tris gels according to the NuPAGE protocol (Novex). Proteins were transferred to PVDF membranes via the iBlot 2 device (Thermo Fisher). Immunoblots were probed with polyclonal rabbit anti-PLA2G7 antibody (1:500, 15526-1-AP, ProteinTech). GAPDH levels were measured as a loading control with a monoclonal mouse anti-GAPDH antibody (1:1,000, sc-32233, Santa Cruz). Donkey anti-rabbit IR800 and donkey anti-mouse IR680 secondary antibodies (1:10,000, LI-COR Biosciences) were used to detect PLA2G7 and GAPDH, respectively. Immunoblots were imaged using a LI-COR Odyssey infrared imager, and relative band intensities were quantified using Image Studio (LI-COR Biosciences).

Human study and sample collection. Clinical sensory data and skin biopsies collected from 12 control participants and 16 participants with type 2 diabetes and diabetic neuropathy (all aged >50 years) were included as part of an ongoing observational trial at the UTHSCSA. Regulatory approval was obtained from the Human Subjects Institutional Review Board at the UTHSCSA (20160027HU). Participant information is available in Supplementary Table 2. Informed consent was obtained from participants according to protocol guidelines set by the Institutional Review Board. Participants completed self-reported pain questionnaires for LANSS and NPSI assessments, followed by sensory testing as previously described[48]. Vibration-detection thresholds were then determined for both halluces for each patient, followed by collection of a skin punch biopsy. Study data were collected and managed using REDCap electronic data-capture tools hosted at the UTHSCSA[90].

For vibration testing, a Rydel-Seiffer tuning fork (US Neurologicals) was used on left and right halluces (that is, great toes). The principal neurologist placed the base of the tuning fork, with dampers facing the researcher, on the bony prominences. To create a vibration, tynes were pressed together between the thumb and the index finger and then released such that the illusion of two triangles was visible on each damper marked on a scale from 0 to 8. As the intensity of the vibration diminished, the two triangles moved closer together and the point of intersection moved slowly upward. Each patient vocalised once the vibration could not be detected, and the intensity score was recorded. This procedure was repeated four times per hallux, with the first reading being discarded and the last three being recorded.

Lastly, following injection with a 2% lidocaine–epinephrine (Hospira) solution to anaesthetise the skin, punch biopsies were taken 10 cm proximal to the lateral malleolus of the ankle to a depth of 4 mm with a sterile 4-mm circular punch. Biopsies were collected in sterile 2-ml cryotubes and immediately snap frozen on liquid nitrogen. Samples were stored at −80 °C until processing for total lipid analysis.

Statistical analysis and reproducibility. Prism 9.0 (GraphPad) was used for statistical analysis. Statistical tests used are specified at the end of each figure legend. Generally, unpaired, two-tailed Student's *t*-tests were used for analyses between two groups, whereas one-way or two-way ANOVA coupled with a specific multiple-comparisons test was used for multiple groups and/or conditions. Sample sizes were designed to generate 80% power at two-sided $P < 0.05$. Unless otherwise specified, data are presented as mean ± s.e.m., with values derived from independent biological replicates. Information pertaining to use of technical replicates can be found in the Methods (for example, qPCR, HPLC–MS/MS, IHC). Results from all experiments that used males and females were tested for possible sex differences, and, if none were observed, animals were combined for further analysis[91]. OmniGraffle version 7.18.1 (the Omni Group) was used for illustrations and figure organisation.

Reporting Summary. Further information on research design is available in the Nature Research Reporting Summary linked to this article.

Data availability

Data that support the findings of this study are available from the corresponding author upon request. Source data are provided with this paper.

Received: 22 December 2020; Accepted: 12 May 2021;
Published online: 17 June 2021

References

1. Vos, T. et al. Global, regional, and national incidence, prevalence, and years lived with disability for 328 diseases and injuries for 195 countries, 1990–2016: a systematic analysis for the Global Burden of Disease Study 2016. *Lancet* **390**, 1211–1259 (2017).
2. Mills, S. E. E., Nicolson, K. P. & Smith, B. H. Chronic pain: a review of its epidemiology and associated factors in population-based studies. *Br. J. Anaesth.* **123**, e273–e283 (2019).
3. Gabbs, M., Leng, S., Devassy, J. G., Monirujjaman, M. & Aukema, H. M. Advances in our understanding of oxylipins derived from dietary PUFAs. *Adv. Nutr.* **6**, 513–540 (2015).
4. Shearer, G. C. & Walker, R. E. An overview of the biologic effects of omega-6 oxylipins in humans. *Prostaglandins Leukot. Essent. Fatty Acids* **137**, 26–38 (2018).
5. Simopoulos, A. P. Evolutionary aspects of diet, the omega-6/omega-3 ratio and genetic variation: nutritional implications for chronic diseases. *Biomed. Pharmacother.* **60**, 502–507 (2006).
6. Mann, J. I. Diet and risk of coronary heart disease and type 2 diabetes. *Lancet* **360**, 783–789 (2002).
7. Manzel, A. et al. Role of 'western diet' in inflammatory autoimmune diseases. *Curr. Allergy Asthma Rep.* **14**, 404 (2014).
8. Blasbalg, T. L., Hibbeln, J. R., Ramsden, C. E., Majchrzak, S. F. & Rawlings, R. R. Changes in consumption of omega-3 and omega-6 fatty acids in the United States during the 20th century. *Am. J. Clin. Nutr.* **93**, 950–962 (2011).
9. Kris-Etherton, P. M. et al. Polyunsaturated fatty acids in the food chain in the United States. *Am. J. Clin. Nutr.* **71**, 179S–188S (2000).
10. Patwardhan, A. M. et al. Heat generates oxidized linoleic acid metabolites that activate TRPV1 and produce pain in rodents. *J. Clin. Invest.* **120**, 1617–1626 (2010).
11. Eskander, M. A. et al. Persistent nociception triggered by nerve growth factor (NGF) is mediated by TRPV1 and oxidative mechanisms. *J. Neurosci.* **35**, 8593–8603 (2015).
12. Green, D. P., Ruparel, S., Roman, L., Henry, M. A. & Hargreaves, K. M. Role of endogenous TRPV1 agonists in a postburn pain model of partial-thickness injury. *Pain* **154**, 2512–2520 (2013).
13. Ramsden, C. E. et al. A systems approach for discovering linoleic acid derivatives that potentially mediate pain and itch. *Sci. Signal.* **10**, eaal5241 (2017).
14. Sisignano, M. et al. Targeting CYP2J to reduce paclitaxel-induced peripheral neuropathic pain. *Proc. Natl Acad. Sci. USA* **113**, 12544–12549 (2016).
15. Clarke, G. et al. Marked elevations in pro-inflammatory polyunsaturated fatty acid metabolites in females with irritable bowel syndrome. *J. Lipid Res.* **51**, 1186–1192 (2010).
16. Adam, O. et al. Anti-inflammatory effects of a low arachidonic acid diet and fish oil in patients with rheumatoid arthritis. *Rheumatol. Int.* **23**, 27–36 (2003).
17. Calder, P. C. Session 3: Joint Nutrition Society and Irish Nutrition and Dietetic Institute Symposium on 'Nutrition and autoimmune disease' PUFA, inflammatory processes and rheumatoid arthritis. *Proc. Nutr. Soc.* **67**, 409–418 (2008).
18. Devigili, G. et al. The diagnostic criteria for small fibre neuropathy: from symptoms to neuropathology. *Brain* **131**, 1912–1925 (2008).
19. Lauria, G. et al. European Federation of Neurological Societies/Peripheral Nerve Society Guideline on the use of skin biopsy in the diagnosis of small fiber neuropathy. Report of a joint task force of the European Federation of Neurological Societies and the Peripheral Nerve Society. *Eur. J. Neurol.* **17**, 903–912 (2010).
20. Hunt, D., Raivich, G. & Anderson, P. N. Activating transcription factor 3 and the nervous system. *Front. Mol. Neurosci.* **5**, 7 (2012).
21. Tsujino, H. et al. Activating transcription factor 3 (ATF3) induction by axotomy in sensory and motoneurons: a novel neuronal marker of nerve injury. *Mol. Cell. Neurosci.* **15**, 170–182 (2000).
22. Bray, G. A. & Popkin, B. M. Dietary fat intake does affect obesity! *Am. J. Clin. Nutr.* **68**, 1157–1173 (1998).
23. Forouhi, N. G. et al. Association of plasma phospholipid *n*-3 and *n*-6 polyunsaturated fatty acids with type 2 diabetes: the EPIC-InterAct case-cohort study. *PLoS Med.* **13**, e1002094 (2016).
24. Fung, T. T., Schulze, M., Manson, J. E., Willett, W. C. & Hu, F. B. Dietary patterns, meat intake, and the risk of type 2 diabetes in women. *Arch. Intern. Med.* **164**, 2235–2240 (2004).
25. Mente, A. et al. Association of dietary nutrients with blood lipids and blood pressure in 18 countries: a cross-sectional analysis from the PURE study. *Lancet Diabetes Endocrinol.* **5**, 774–787 (2017).
26. van Dam, R. M., Willett, W. C., Rimm, E. B., Stampfer, M. J. & Hu, F. B. Dietary fat and meat intake in relation to risk of type 2 diabetes in men. *Diabetes Care* **25**, 417–424 (2002).
27. Ramsden, C. E. et al. Dietary linoleic acid-induced alterations in pro- and anti-nociceptive lipid autacoids: implications for idiopathic pain syndromes? *Mol. Pain* **12**, 1744806916636386 (2016).

28. Patwardhan, A. M., Scotland, P. E., Akopian, A. N. & Hargreaves, K. M. Activation of TRPV1 in the spinal cord by oxidized linoleic acid metabolites contributes to inflammatory hyperalgesia. *Proc. Natl Acad. Sci. USA* **106**, 18820–18824 (2009).
29. Griffin, T. M. et al. Diet-induced obesity differentially regulates behavioral, biomechanical, and molecular risk factors for osteoarthritis in mice. *Arthritis Res. Ther.* **12**, R130 (2010).
30. Lee, E. et al. Transient receptor potential vanilloid type-1 channel regulates diet-induced obesity, insulin resistance, and leptin resistance. *FASEB J.* **29**, 3182–3192 (2015).
31. Tramullas, M., Finger, B. C., Dinan, T. G. & Cryan, J. F. Obesity takes its toll on visceral pain: high-fat diet induces Toll-like receptor 4-dependent visceral hypersensitivity. *PLoS ONE* **11**, e0155367 (2016).
32. Wilensky, R. L. et al. Inhibition of lipoprotein-associated phospholipase A2 reduces complex coronary atherosclerotic plaque development. *Nat. Med.* **14**, 1059–1066 (2008).
33. Wallace, V. C., Cottrell, D. F., Brophy, P. J. & Fleetwood-Walker, S. M. Focal lysolecithin-induced demyelination of peripheral afferents results in neuropathic pain behavior that is attenuated by cannabinoids. *J. Neurosci.* **23**, 3221–3233 (2003).
34. Piomelli, D. & Sasso, O. Peripheral gating of pain signals by endogenous lipid mediators. *Nat. Neurosci.* **17**, 164–174 (2014).
35. Dennis, E. A., Cao, J., Hsu, Y. H., Magrioti, V. & Kokotos, G. Phospholipase A2 enzymes: physical structure, biological function, disease implication, chemical inhibition, and therapeutic intervention. *Chem. Rev.* **111**, 6130–6185 (2011).
36. Usoskin, D. et al. Unbiased classification of sensory neuron types by large-scale single-cell RNA sequencing. *Nat. Neurosci.* **18**, 145–153 (2015).
37. Kim, M. et al. Impact of 8-week linoleic acid intake in soy oil on Lp-PLA2 activity in healthy adults. *Nutr. Metab.* **14**, 32 (2017).
38. Blackie, J. A. et al. The identification of clinical candidate SB-480848: a potent inhibitor of lipoprotein-associated phospholipase A2. *Bioorg. Med. Chem. Lett.* **13**, 1067–1070 (2003).
39. Goldberg, R. J. & Katz, J. A meta-analysis of the analgesic effects of omega-3 polyunsaturated fatty acid supplementation for inflammatory joint pain. *Pain* **129**, 210–223 (2007).
40. Laye, S., Nadjar, A., Joffre, C. & Bazinet, R. P. Anti-inflammatory effects of omega-3 fatty acids in the brain: physiological mechanisms and relevance to pharmacology. *Pharmacol. Rev.* **70**, 12–38 (2018).
41. Xu, Z. Z. et al. Resolvins RvE1 and RvD1 attenuate inflammatory pain via central and peripheral actions. *Nat. Med.* **16**, 592–597 (2010).
42. Bazata, D. D., Robinson, J. G., Fox, K. M., Grandy, S. & Group, S. S. Affecting behavior change in individuals with diabetes: findings from the Study to Help Improve Early Evaluation and Management of Risk Factors Leading to Diabetes (SHIELD). *Diabetes Educ.* **34**, 1025–1036 (2008).
43. Davis, J. A., Robinson, R. L., Le, T. K. & Xie, J. Incidence and impact of pain conditions and comorbid illnesses. *J. Pain Res.* **4**, 331–345 (2011).
44. Fehrenbacher, J. C., Vasko, M. R. & Duarte, D. B. Models of inflammation: carrageenan- or complete Freund's adjuvant (CFA)-induced edema and hypersensitivity in the rat. *Curr. Protoc. Pharmacol.* **56**, 5.4 (2012).
45. Kobayashi, K. et al. The db/db mouse, a model for diabetic dyslipidemia: molecular characterization and effects of Western diet feeding. *Metabolism* **49**, 22–31 (2000).
46. O'Brien, P. D., Sakowski, S. A. & Feldman, E. L. Mouse models of diabetic neuropathy. *ILAR J.* **54**, 259–272 (2014).
47. Alvheim, A. R. et al. Dietary linoleic acid elevates endogenous 2-AG and anandamide and induces obesity. *Obesity* **20**, 1984–1994 (2012).
48. Bennett, M. The LANSS Pain Scale: the Leeds assessment of neuropathic symptoms and signs. *Pain* **92**, 147–157 (2001).
49. Bouhassira, D. et al. Development and validation of the Neuropathic Pain Symptom Inventory. *Pain* **108**, 248–257 (2004).
50. Mauck, M. C. et al. Obesity increases the risk of chronic pain development after motor vehicle collision. *Pain* **160**, 670–675 (2019).
51. Okifuji, A. & Hare, B. D. The association between chronic pain and obesity. *J. Pain Res.* **8**, 399–408 (2015).
52. White, H. D. et al. Darapladib for preventing ischemic events in stable coronary heart disease. *N. Engl. J. Med.* **370**, 1702–1711 (2014).
53. O'Donoghue, M. L. et al. Effect of darapladib on major coronary events after an acute coronary syndrome: the SOLID-TIMI 52 randomized clinical trial. *JAMA* **312**, 1006–1015 (2014).
54. Haghdoost, F. et al. Association between Ala379Val polymorphism of lipoprotein-associated phospholipase A2 and migraine without aura in Iranian population. *Iran. J. Neurol.* **15**, 80–84 (2016).
55. Parisien, M. et al. Effect of human genetic variability on gene expression in dorsal root ganglia and association with pain phenotypes. *Cell Rep.* **19**, 1940–1952 (2017).
56. Hummel, K. P., Dickie, M. M. & Coleman, D. L. Diabetes, a new mutation in the mouse. *Science* **153**, 1127–1128 (1966).
57. Reeves, P. G., Nielsen, F. H. & Fahey, G. C. Jr. AIN-93 purified diets for laboratory rodents: final report of the American Institute of Nutrition ad hoc writing committee on the reformulation of the AIN-76A rodent diet. *J. Nutr.* **123**, 1939–1951 (1993).
58. Gibbs, J. L., Flores, C. M. & Hargreaves, K. M. Attenuation of capsaicin-evoked mechanical allodynia by peripheral neuropeptide Y Y_1 receptors. *Pain* **124**, 167–174 (2006).
59. Chaplan, S. R., Bach, F. W., Pogrel, J. W., Chung, J. M. & Yaksh, T. L. Quantitative assessment of tactile allodynia in the rat paw. *J. Neurosci. Methods* **53**, 55–63 (1994).
60. White, S., Marquez de Prado, B., Russo, A. F. & Hammond, D. L. Heat hyperalgesia and mechanical hypersensitivity induced by calcitonin gene-related peptide in a mouse model of neurofibromatosis. *PLoS ONE* **9**, e106767 (2014).
61. Garrison, S. R., Dietrich, A. & Stucky, C. L. TRPC1 contributes to light-touch sensation and mechanical responses in low-threshold cutaneous sensory neurons. *J. Neurophysiol.* **107**, 913–922 (2012).
62. Hargreaves, K., Dubner, R., Brown, F., Flores, C. & Joris, J. A new and sensitive method for measuring thermal nociception in cutaneous hyperalgesia. *Pain* **32**, 77–88 (1988).
63. Brenner, D. S., Golden, J. P. & Gereau, R. W. T. A novel behavioral assay for measuring cold sensation in mice. *PLoS ONE* **7**, e39765 (2012).
64. Ayala, J. E. et al. Standard operating procedures for describing and performing metabolic tests of glucose homeostasis in mice. *Dis. Model. Mech.* **3**, 525–534 (2010).
65. Han, B. G. et al. Markers of glycemic control in the mouse: comparisons of 6-h- and overnight-fasted blood glucoses to Hb A1c. *Am. J. Physiol. Endocrinol. Metab.* **295**, E981–E986 (2008).
66. Wang, M. & Han, X. Multidimensional mass spectrometry-based shotgun lipidomics. *Methods Mol. Biol.* **1198**, 203–220 (2014).
67. Han, X., Yang, K. & Gross, R. W. Microfluidics-based electrospray ionization enhances the intrasource separation of lipid classes and extends identification of individual molecular species through multi-dimensional mass spectrometry: development of an automated high-throughput platform for shotgun lipidomics. *Rapid Commun. Mass Spectrom.* **22**, 2115–2124 (2008).
68. Wang, M., Wang, C., Han, R. H. & Han, X. Novel advances in shotgun lipidomics for biology and medicine. *Prog. Lipid Res.* **61**, 83–108 (2016).
69. Yang, K., Cheng, H., Gross, R. W. & Han, X. Automated lipid identification and quantification by multidimensional mass spectrometry-based shotgun lipidomics. *Anal. Chem.* **81**, 4356–4368 (2009).
70. Bligh, E. G. & Dyer, W. J. A rapid method of total lipid extraction and purification. *Can. J. Biochem. Physiol.* **37**, 911–917 (1959).
71. Pettinella, C., Lee, S. H., Cipollone, F. & Blair, I. A. Targeted quantitative analysis of fatty acids in atherosclerotic plaques by high sensitivity liquid chromatography/tandem mass spectrometry. *J. Chromatogr. B Analyt. Technol. Biomed. Life Sci.* **850**, 168–176 (2007).
72. Quehenberger, O., Armando, A. M. & Dennis, E. A. High sensitivity quantitative lipidomics analysis of fatty acids in biological samples by gas chromatography–mass spectrometry. *Biochim. Biophys. Acta* **1811**, 648–656 (2011).
73. Reeh, P. W. Sensory receptors in a mammalian skin-nerve in vitro preparation. *Prog. Brain Res.* **74**, 271–276 (1988).
74. Banik, R. K. & Brennan, T. J. Sensitization of primary afferents to mechanical and heat stimuli after incision in a novel in vitro mouse glabrous skin-nerve preparation. *Pain* **138**, 380–391 (2008).
75. Zimmermann, K. et al. Phenotyping sensory nerve endings in vitro in the mouse. *Nat. Protoc.* **4**, 174–196 (2009).
76. Hogan, D., Baker, A. L., Moron, J. A. & Carlton, S. M. Systemic morphine treatment induces changes in firing patterns and responses of nociceptive afferent fibers in mouse glabrous skin. *Pain* **154**, 2297–2309 (2013).
77. Moehring, F. et al. Keratinocytes mediate innocuous and noxious touch via ATP–P2X4 signaling. *eLife* **7**, e31684 (2018).
78. Duraku, L. S. et al. Spatiotemporal dynamics of re-innervation and hyperinnervation patterns by uninjured CGRP fibers in the rat foot sole epidermis after nerve injury. *Mol. Pain* **8**, 61 (2012).
79. Reid, G., Amuzescu, B., Zech, E. & Flonta, M. L. A system for applying rapid warming or cooling stimuli to cells during patch clamp recording or ion imaging. *J. Neurosci. Methods* **111**, 1–8 (2001).
80. Koltzenburg, M., Stucky, C. L. & Lewin, G. R. Receptive properties of mouse sensory neurons innervating hairy skin. *J. Neurophysiol.* **78**, 1841–1850 (1997).
81. Banik, R. K. & Brennan, T. J. Spontaneous discharge and increased heat sensitivity of rat C-fiber nociceptors are present in vitro after plantar incision. *Pain* **112**, 204–213 (2004).
82. Collins, T. J. ImageJ for microscopy. *Biotechniques* **43**, 25–30 (2007).
83. Linkert, M. et al. Metadata matters: access to image data in the real world. *J. Cell Biol.* **189**, 777–782 (2010).
84. Schindelin, J. et al. Fiji: an open-source platform for biological-image analysis. *Nat. Methods* **9**, 676–682 (2012).

85. Schneider, C. A., Rasband, W. S. & Eliceiri, K. W. NIH Image to ImageJ: 25 years of image analysis. *Nat. Methods* **9**, 671–675 (2012).
86. LoCoco, P. M. et al. Pharmacological augmentation of nicotinamide phosphoribosyltransferase (NAMPT) protects against paclitaxel-induced peripheral neuropathy. *eLife* **6**, e29626 (2017).
87. Beiswenger, K. K., Calcutt, N. A. & Mizisin, A. P. Epidermal nerve fiber quantification in the assessment of diabetic neuropathy. *Acta Histochem.* **110**, 351–362 (2008).
88. LoCoco, P. M. et al. Reliable approaches to extract high-integrity RNA from skin and other pertinent tissues used in pain research. *Pain Rep.* **5**, e818 (2020).
89. Livak, K. J. & Schmittgen, T. D. Analysis of relative gene expression data using real-time quantitative PCR and the $2^{-\Delta\Delta C(T)}$ method. *Methods* **25**, 402–408 (2001).
90. Harris, P. A. et al. Research electronic data capture (REDCap)—a metadata-driven methodology and workflow process for providing translational research informatics support. *J. Biomed. Inform.* **42**, 377–381 (2009).
91. Beery, A. K. Inclusion of females does not increase variability in rodent research studies. *Curr. Opin. Behav. Sci.* **23**, 143–149 (2018).

Acknowledgements

The project described was supported in part by the National Center for Advancing Translational Sciences, National Institutes of Health (NIH), through grant UL1TR002645 (K.M.H.). Additional support from the NIH includes grants R01NS110948 (K.M.H.), T32DE14318 (P.M.L., A.R.F., K.M.H.), T32GM113896 (J.T.B.), F30AT009949 (J.T.B.), F32DK118841 (P.M.L.), F30DE028486 (A.R.F.) and a grant from the Ella and Williams Owen's Foundation (K.M.H.). Clinical data were managed using REDCap software supported by UL1RR024982. Certain mass spectrometric analyses were carried out on equipment supported by the US Department of Agriculture, Agricultural Research Service, under agreement no. 58-3094-8-012. The content is solely the responsibility of the authors and does not necessarily represent the official views of the NIH or the US Department of Agriculture. We thank X. Han and his laboratory for expertise and guidance on shotgun lipidomics. We thank M. Patil and P. Wu for technical assistance as well as A. Diogenes, N. Ruparel, A. Khan and A. Akopian for fruitful discussions.

Author contributions

J.T.B., P.M.L., S.B.R. and K.M.H. conceived and designed the studies; J.T.B., P.M.L., M.R.B. and M.T. conducted behavioural experiments; A.R.F., P.M.L. and F.-M.C. conducted single-fibre electrophysiology; P.M.L. and J.T.B. performed histology; Q.L., F.-M.C. and P.M.L. performed BODIPY experiments; P.M.L., D.A.A. and M.T. performed total tissue lipid extractions; M.E.C., G.M.S. and S.B.H.B. conducted quantitative LC–MS/MS; P.M.L. and F.-M.C. performed western blots; E.E.L. and A.T. conducted neurological assessments on trial participants and collected skin punch biopsies; J.T.B., P.M.L. and K.M.H. performed data analysis for all experiments; P.M.L. and J.T.B. prepared figures, images and illustrations; P.M.L., J.T.B. and K.M.H. wrote the manuscript; all authors revised the manuscript.

Competing interests

The authors declare no competing interests.

Additional information

Extended data is available for this paper at https://doi.org/10.1038/s42255-021-00410-x.

Supplementary information The online version contains supplementary material available at https://doi.org/10.1038/s42255-021-00410-x.

Correspondence and requests for materials should be addressed to K.M.H.

Peer review information *Nature Metabolism* thanks Jing Kang, Ru-Rong Ji and the other, anonymous, reviewer(s) for their contribution to the peer review of this work. Primary Handling Editor: Christoph Schmitt.

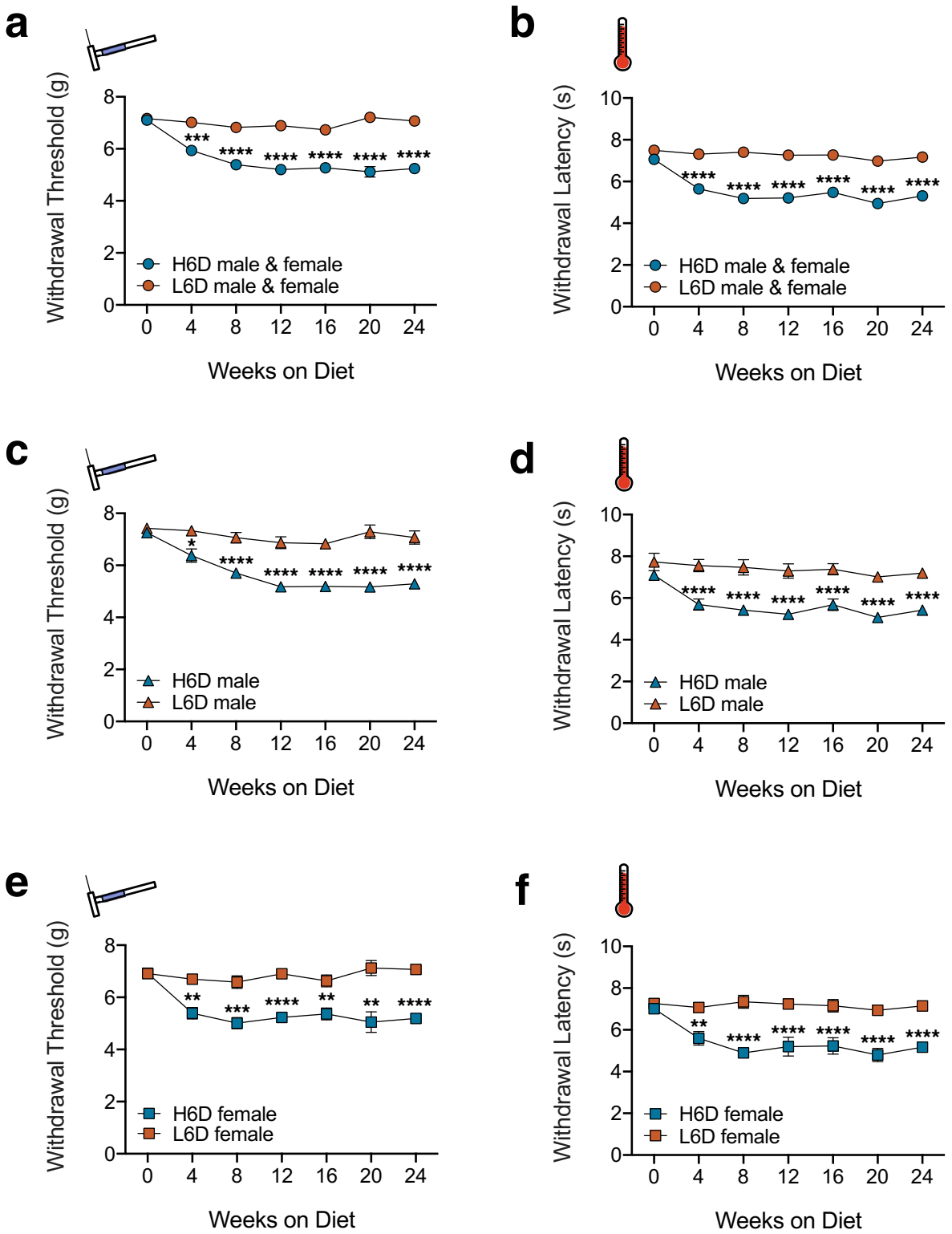

Extended Data Fig. 1 | H6D induces persistent nociceptive hypersensitivities in both male and female mice. a-f, Time courses of changes in mechanical withdrawal threshold (**a**,**c**,**e**) and heat withdrawal latency (**b**,**d**,**f**) for male and female mice on the H6D and L6D. The top two plots (**a**,**b**) represent compiled male and female responses (L6D, n = 24; H6D, n = 29). **a**, ***P = 0.0003 week 4, ****P < 0.0001 weeks 8–24. **b**, ****P < 0.0001 weeks 4–24. The middle plots (**c**,**d**) are male-only responses (L6D, n = 12; H6D, n = 16). **c**, *P = 0.0401 week 4, ****P < 0.0001 weeks 8–24. **d**, ****P < 0.0001 weeks 4–24. The bottom plots (**e**,**f**) are female-only responses (L6D, n = 12; H6D, n = 13). **e**, **P = 0.0055 week 16, 0.0023 week 20, ***P = 0.0009 week 4, 0.0005 week 8, ****P < 0.0001 weeks 12,24. **f**, **P = 0.0022 week 4, ****P < 0.0001 weeks 8–24. Data are mean ± SEM. Error bars for some data points are within the size of the symbol. The statistical test used was two-way repeated-measures ANOVA with Sidak's post-hoc test (**a**-**f**).

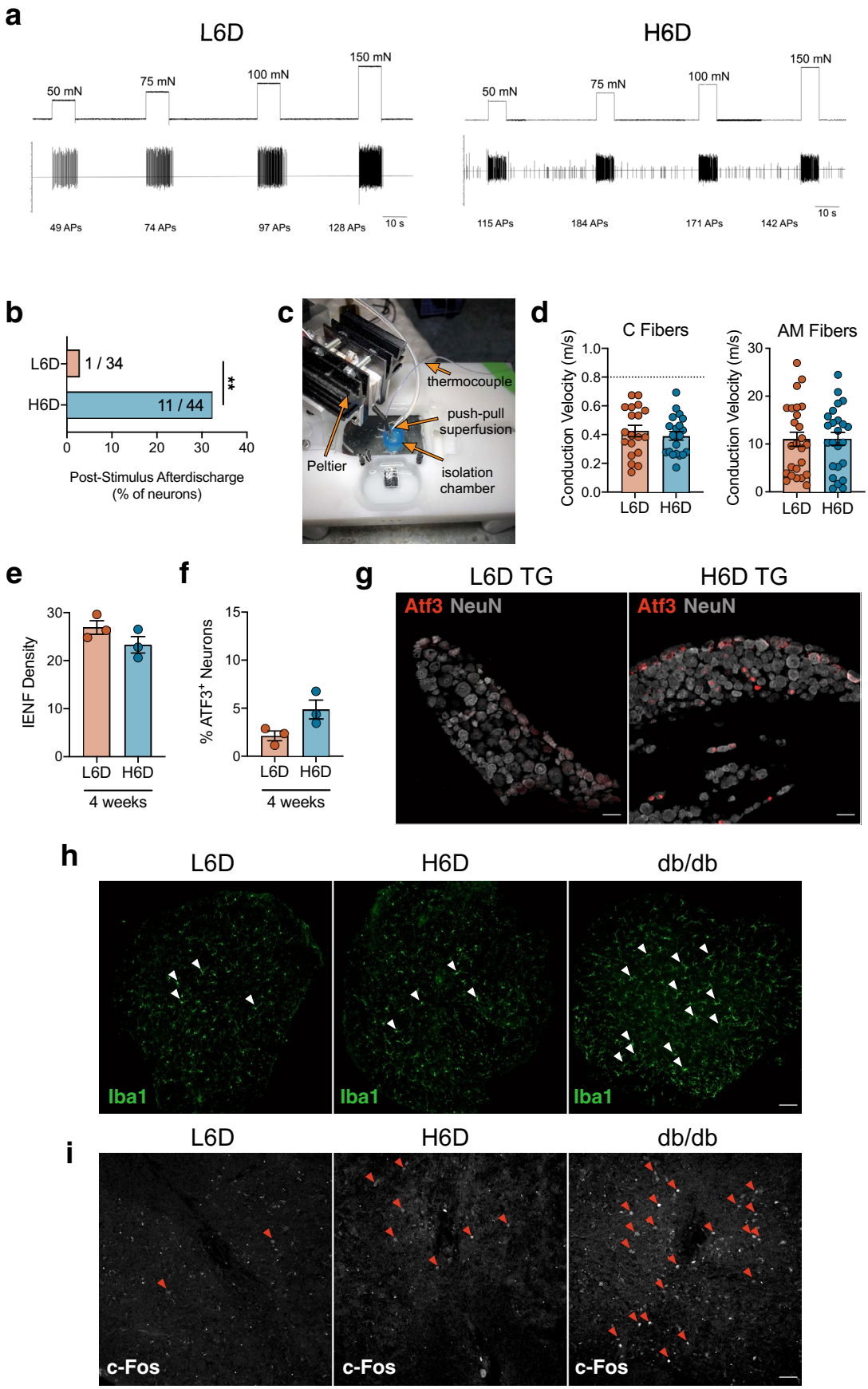

Extended Data Fig. 2 | See next page for caption.

Extended Data Fig. 2 | The H6D sensitizes afferent fibers to mechanical and heat stimuli. a, Representative recording wavemarks from L6D and H6D mice during mechanical force application. The number of action potentials are denoted beneath each stimulation for each recording. **b**, Percentage of fibers exhibiting post-stimulus afterdischarge following mechanical force application. Values represent the number of fibers exhibiting afterdischarge over the total recorded fibers for each group (L6D, n = 34; H6D, n = 44). **P = 0.0096. **c**, The Peltier-based heat delivery system setup. **d**, Conduction velocities determined for recorded C (left) and AM (right) fibers from L6D and H6D mice (L6D-C, n = 19; H6D-C, n = 20; L6D-AM, n = 25; H6D-AM, n = 24). Dotted line represents cut-off value for C fiber classification. **e**,**f**, Glabrous IENF densities (**e**) and percentage of $ATF3^+$ neurons in lumbar DRG (**f**) after 4 weeks on the L6D or H6D (L6D, n = 3; H6D, n = 3). **g**, Representative immunofluorescent staining of ATF3 expression in trigeminal ganglia (TG) from L6D and H6D mice co-localized with NeuN, scale bars: 50 µm (n = 2 mice/group). **h**,**i**, Immunofluorescent staining of Iba1 (**h**) and c-Fos (**i**) expression in the lumbar spinal cord of L6D and H6D mice. Positive control tissue was utilized from db/db mice. White arrowheads designate microglia (**h**), 10X magnification, scale bar: 50 µm (n = 2 mice/group). Red arrowheads designate $c\text{-}Fos^+$ nuclei (**i**), 20X magnification, scale bar: 50 µm (n = 2 mice/group). All data are mean ± SEM. The statistical test used was a two-sided Fisher's exact test (**b**).

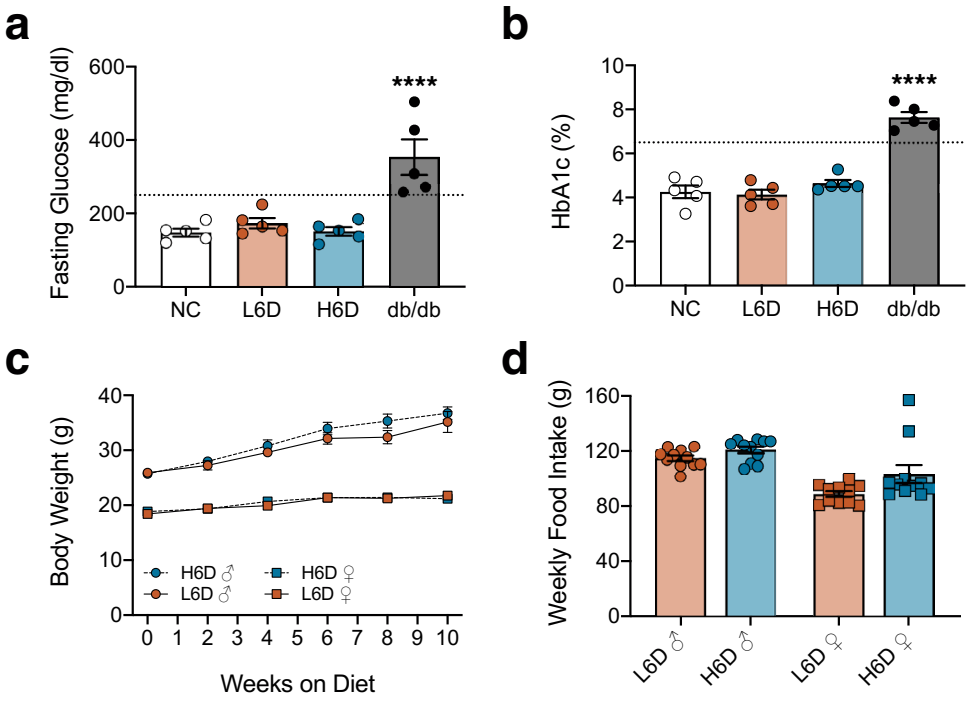

Extended Data Fig. 3 | The H6D does not induce a diabetic phenotype. a,**b**, Scatter plots of fasting blood glucose levels (**a**) and HbA1c levels (**b**) from mice on L6D and H6D for 8 weeks. Mice on normal chow (NC) and 16-week-old db/db mice served as negative and positive controls, respectively (NC, n = 5; L6D, n = 5; H6D, n = 5; db/db, n = 5). Dotted lines in each figure represent established cut-offs for type 2 diabetes. ****$P < 0.0001$ (db/db vs NC). **c**,**d**, Weekly monitoring of body weights (**c**) and food intake (**d**) for both male and female mice on either L6D or H6D. Data are mean ± SEM. Error bars for some data points are within the size of the symbol. Statistical test used was one-way ANOVA with Tukey's post-hoc test (**a**,**b**).

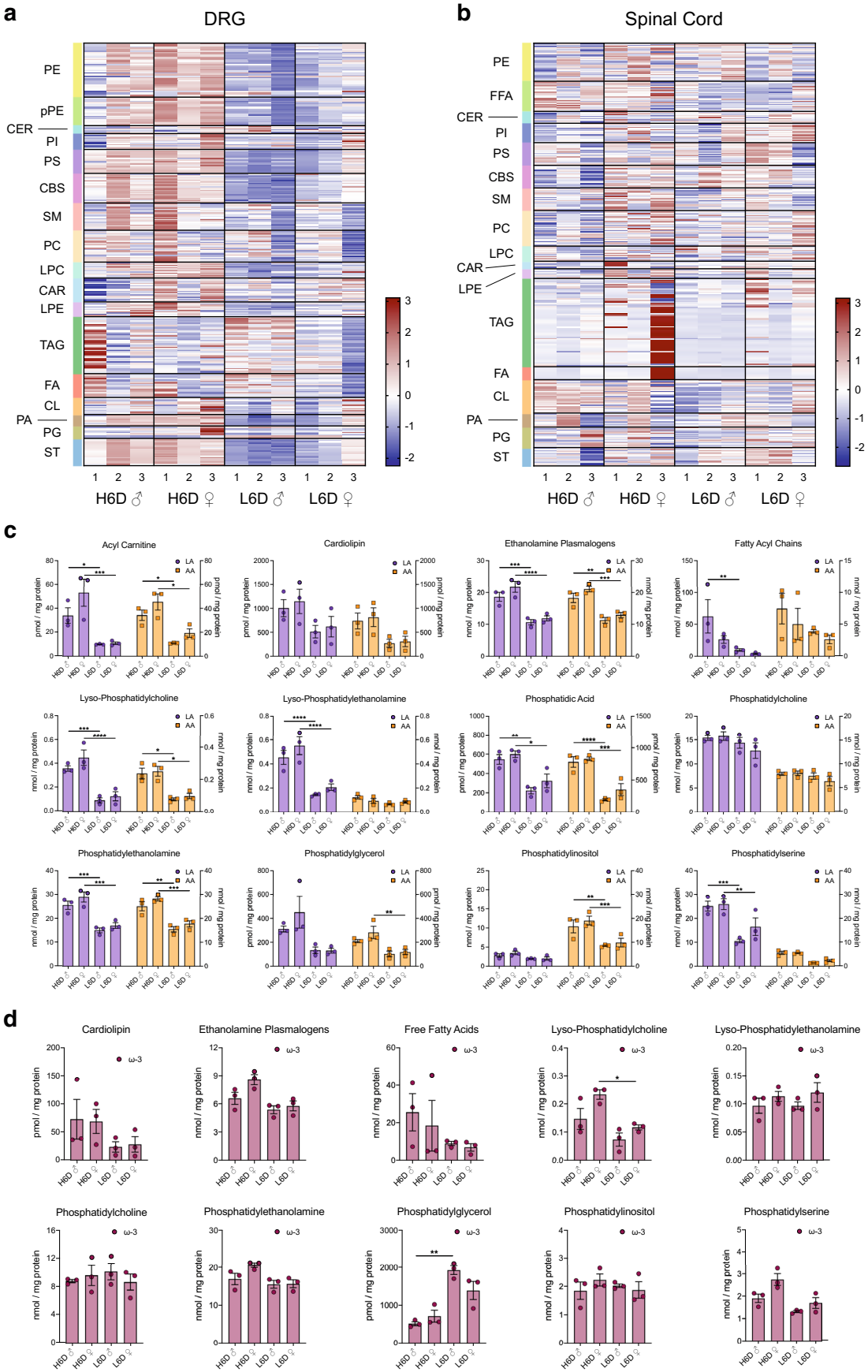

Extended Data Fig. 4 | See next page for caption.

Extended Data Fig. 4 | The H6D alters lipid composition in DRG, but not spinal cord. a,**b**, Heatmaps of lipid species from lumbar DRG (**a**) and spinal cord (**b**) from male (♂) and female (♀) mice on either the H6D or L6D. Lipid classes are designated to the left of each heatmap. Scale bar represents z-score transformations for each lipid species. **c**,**d**, Scatter plots of LA- and AA-esterified lipids (**c**) as well as ω-3 content (**d**, EPA, DHA levels) in DRG sub-profiled by lipid class for male and female mice on either diet (n = 3 mice/group/sex). **c**, Acyl carnitine (LA): *P = 0.0346, ***P = 0.0004. Acyl carnitine (AA): *P = 0.0417 (♂), *P = 0.0214 (♀). Ethanolamine plasmalogens (LA): ***P = 0.0008, ****P < 0.0001. Ethanolamine plasmalogens (AA): **P = 0.0027, ***P = 0.0007. Fatty acyl chains (LA): **P = 0.0069. Lyso-phosphatidylcholine (LA): ***P = 0.0002, ****P < 0.0001. Lyso-phosphatidylcholine (AA): *P = 0.0161, *P = 0.0215. Lyso-phosphatidylethanolamine (LA): ****P < 0.0001. Phosphatidic acid (LA): **P = 0.005, *P = 0.0166. Phosphatidic acid (AA): ****P < 0.0001, ***P = 0.0001. Phosphatidylethanolamine (LA): ***P = 0.0006, ***P = 0.0002. Phosphatidylethanolamine (AA): **P = 0.0015, ***P = 0.0007. Phosphatidylglycerol (AA): **P = 0.0033. Phosphatidylinositol (AA): **P = 0.003, ***P = 0.001. Phosphatidylserine (LA): ***P = 0.0001, **P = 0.0072. **d**, Lyso-phosphatidylcholine: *P = 0.0316. Phosphatidylglycerol: **P = 0.0062. Data are mean ± SEM. Statistical tests used were two-way ANOVA with Tukey's post-hoc test (**c**) and one-way ANOVA with Tukey's post-hoc test (**d**).

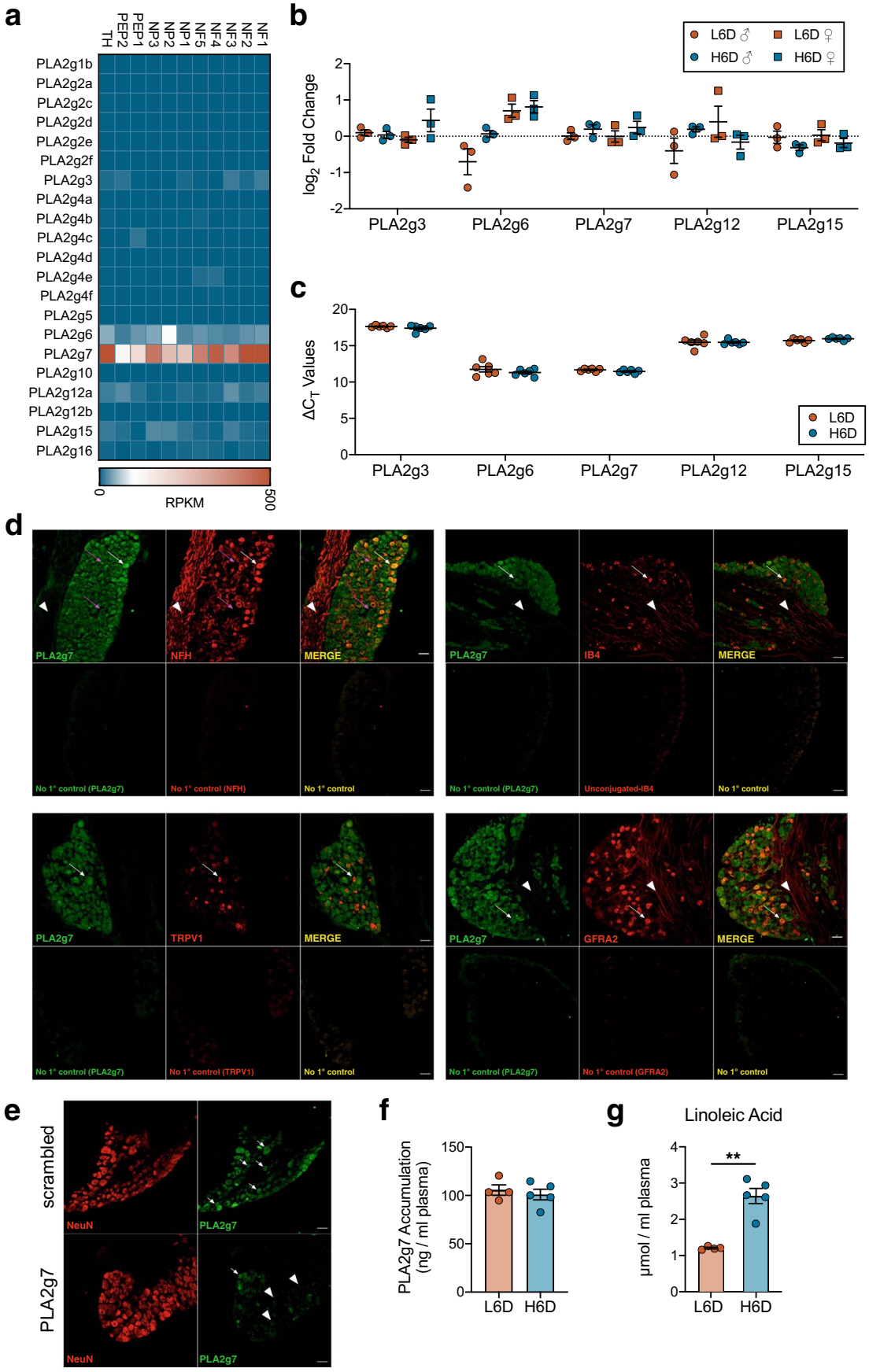

Extended Data Fig. 5 | See next page for caption.

Extended Data Fig. 5 | PLA2g7 expression predominates in neuronal subpopulations of the lumbar DRG. a, Heatmap indicating PLA2 isozyme expression across established neuronal subpopulations of the mouse lumbar DRG. Single-cell RNA-seq data were reproduced with permission[36]. **b**,**c**, qPCR data showing PLA2 isozyme expression (**b**) and change in cycle threshold values relative to 18 S rRNA (**c**) in lumbar DRG from H6D and L6D mice (**b**: n = 3/group. **c**: L6D, n = 6; H6D, n = 6). **d**, Representative immunofluorescent staining of PLA2g7 expression in mouse lumbar DRG and co-localization with neuronal subtype-specific markers. No primary controls are included for each marker as designated. The magenta arrows highlight two small diameter neurons, one with high PLA2g7 expression and one with low to moderate expression, that are negative for NFH. White arrows designate cell bodies with PLA2g7$^+$ staining and their co-localization with the respective subtype marker. White arrowheads highlight axons projecting through the ganglia that exhibit virtually no PLA2g7 expression compared to cell bodies. Scale bars: 50 µm (n = 2 mice). **e**, Representative immunofluorescent staining of lumbar DRG from naïve control mice that received either scrambled or PLA2g7-directed siRNA intrathecally for the purpose of PLA2g7 antibody validation. White arrows highlight PLA2g7 + staining of neuronal cell bodies, whereas the white arrowheads designate cells exhibiting loss of PLA2g7 immunoreactivity. Scale bars: 50 µm, (n = 2 mice/group). **f**,**g**, Circulating plasma PLA2g7 levels (**f**) and plasma LA accumulation (**g**) from L6D and H6D mice after 8 weeks (L6D, n = 4; H6D, n = 5). **P < 0.0022. Data are mean ± SEM. Error bars for some data points are within the size of the symbol. Statistical test used was unpaired two-tailed Student's t test (**g**).

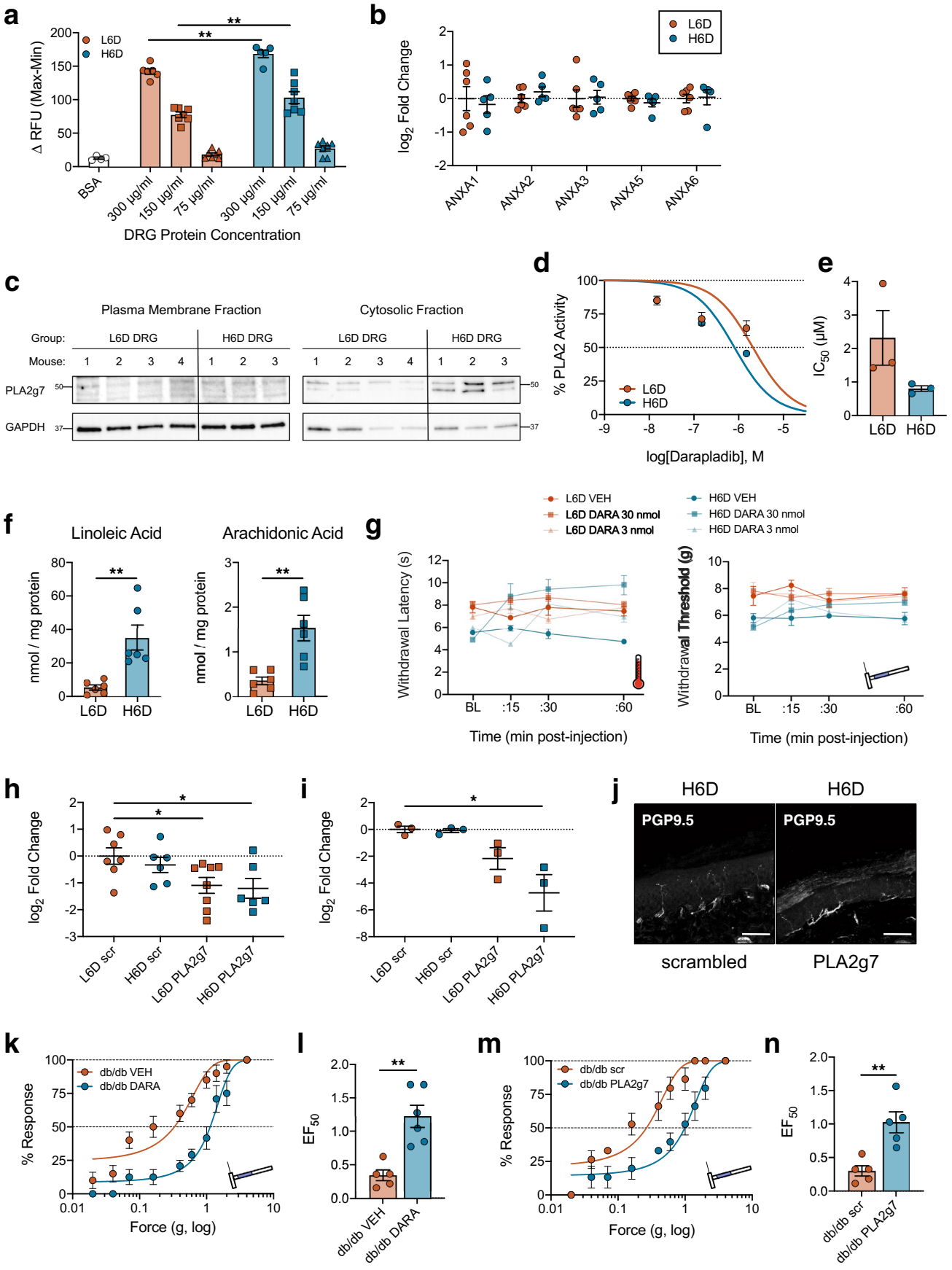

Extended Data Fig. 6 | See next page for caption.

Extended Data Fig. 6 | Pharmacological inhibition and genetic knockdown of PLA2g7 in DRG neurons reduces PLA2 activity and attenuates nociceptive hypersensitivities. a, Optimization of DRG protein concentration used with the PLA2 BODIPY activity assay. H6D DRG homogenates demonstrate increased activity at multiple concentrations compared to L6D (BSA, n = 4; L6D-300, n = 6; L6D-150, n = 7; L6D-75, n = 7; H6D-300, n = 5; H6D-150, n = 7; H6D-75, n = 7 DRG replicates/group). **P = 0.0055 (300), 0.0023 (150). **b**, qPCR data showing annexin isozyme expression in L6D and H6D DRG (L6D, n = 6; H6D, n = 5). **c**, Immunoblots of PLA2g7 and GAPDH protein expression in membrane and cytosolic fractions from homogenized DRG (L6D, n = 4 mice; H6D, n = 3 mice). Molecular weight markers (kDa) are adjacent to each target. **d**, Concentration-response curves for darapladib-mediated inhibition of PLA2 activity for DRG (n = 3/group). **e**, Darapladib half-maximal inhibitory concentrations (IC_{50}) as determined by nonlinear regression (n = 3/group). **f**, Total LA and AA levels determined from glabrous hindpaw skin punches (L6D, n = 6; H6D, n = 6). **P = 0.0098 (LA), 0.0071 (AA). **g**, Dose-response timecourses for i.pl. darapladib on heat- and mechanical-evoked nociception (L6D-VEH, n = 6; L6D-3, n = 4; L6D-30, n = 9; H6D-VEH, n = 6; H6D-3, n = 5; H6D-30, n = 9). **h**,**i**, PLA2g7 qPCR data for lumbar DRG (**h**) and spinal cord (**i**) following intrathecal siRNA treatment (q.d. x 3d) (**h**: L6D-scr, n = 7; H6D-scr, n = 6; L6D-PLA2g7, n = 8; H6D-PLA2g7, n = 6. **i**: n = 3/group). **h**, *P = 0.0429 (L6D-PLA2g7), 0.0371 (H6D-PLA2g7). **i**, *P = 0.0333. **j**, Immunofluorescent images of glabrous IENFs from siRNA-treated mice, scale bar: 50 μm (n = 2 mice/group). **k**,**l**, Mechanical force-response curves (**k**) and EF_{50} values (**l**) for 16-week db/db mice injected i.pl. with either vehicle or darapladib (db/db-veh, n = 5; db/db-DARA, n = 6). **l**, **P = 0.0020. **m**,**n**, Mechanical force-response curves (**m**) and EF_{50} values (**n**) for a different cohort of 16-week db/db mice following i.t. siRNA injections (db/db-veh, n = 5; db/db-darapladib, n = 5). **n**, **P = 0.0066. All data are mean ± SEM. Error bars for some data points are within the size of the symbol. Statistical tests used were one-way ANOVA with Sidak's post-hoc test (**a**), Tukey's post-hoc test (**d**), or Dunnett's post-hoc test (**h**,**i**), two-way ANOVA with Tukey's post-hoc test (**c**), and unpaired two-tailed Student's t test (**f**,**l**,**n**).

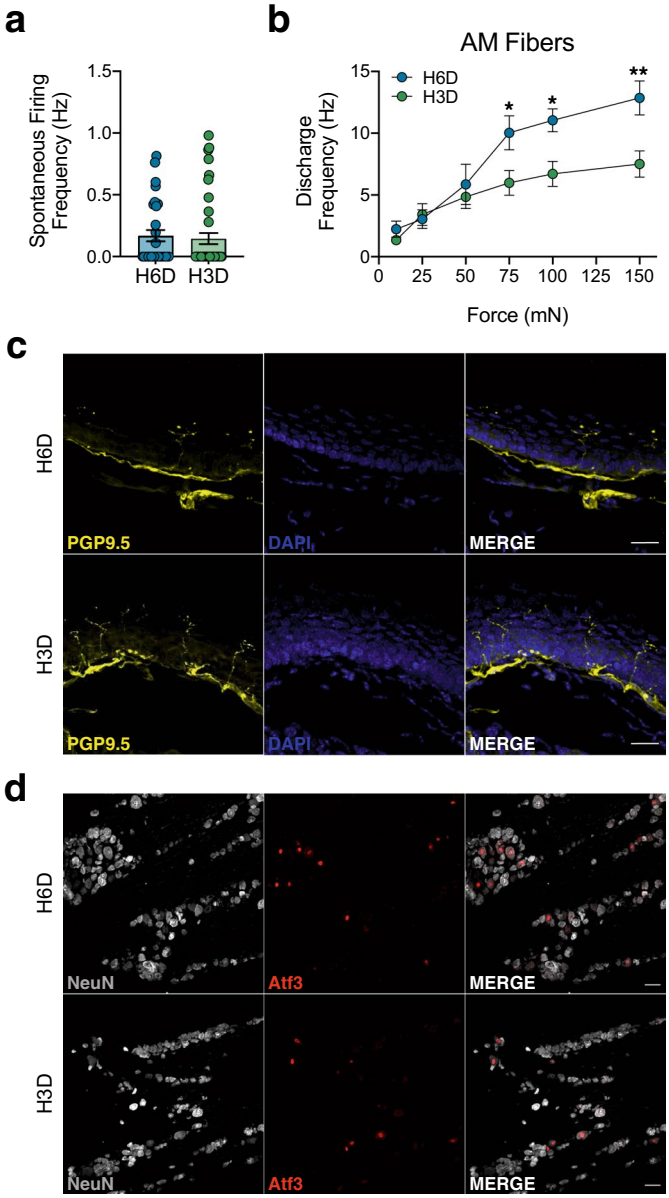

Extended Data Fig. 7 | H3D reverses H6D-induced changes in afferent fibers. a, Discharge frequencies of spontaneously-active fibers (H6D, n = 30; H3D, n = 41). **b**, Discharge frequencies of AM fibers (H6D, n = 13; H3D, n = 21). *P = 0.0353 (75), 0.0335 (100), **P = 0.0047 (150). **c**,**d**, Representative immunofluorescence staining of glabrous hindpaw skin IENFs (**c**) and ATF3 expression in lumbar DRG neurons (**d**) in H6D and H3D mice. Scale bars: 25 µm (**c**; n = 4 mice/group), 50 µm (**d**; n = 3 mice/group). The representative images supplement Figs. 3h and 3i, respectively. Data are mean ± SEM. Error bars for some data points are within the size of the symbol. Statistical test used was two-way ANOVA with Sidak's post-hoc test (**b**).

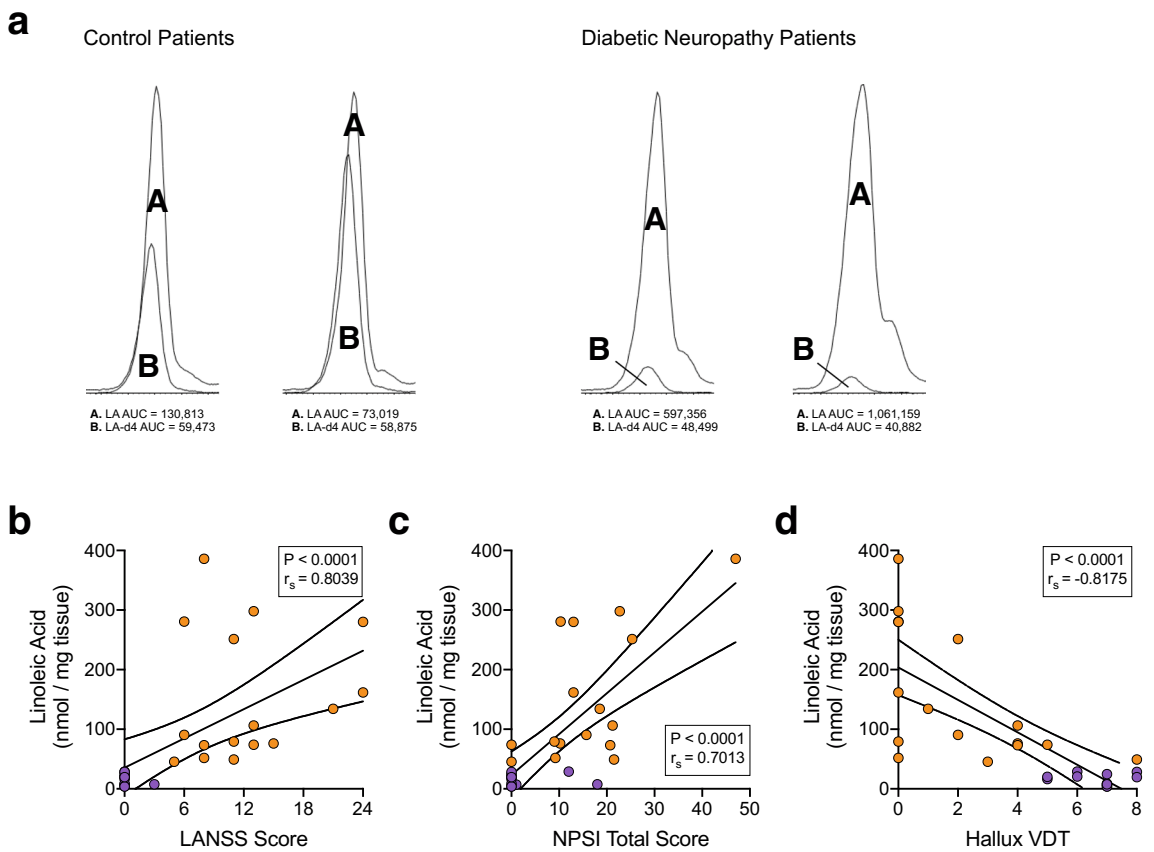

Extended Data Fig. 8 | Increased LA content in skin of diabetic subjects with painful neuropathy. a, Chromatogram snapshots of the endogenous LA peak (labeled A) overlaid with the LA-d_4 internal control peak (labeled B) for skin biopsy extracts from diabetic and control subjects. Integrated AUC values (a.u.) for each peak are beneath each chromatogram. **b**-**d**, Correlation analyses between subject skin LA levels and their respective LANSS scores (**b**), NPSI scores (**c**), and hallux vibration detection thresholds (**d**) (control, n = 12; diabetic, n = 16). Linear regression identified the best-fit line (solid line) with 95% confidence intervals (dotted lines). Inset boxes contain Spearman coefficients (r_s) and corresponding P-values. Statistical test used was two-tailed Spearman correlation.

nature research

Corresponding author(s): Kenneth M. Hargreaves

Last updated by author(s): Apr 26, 2021

Reporting Summary

Nature Research wishes to improve the reproducibility of the work that we publish. This form provides structure for consistency and transparency in reporting. For further information on Nature Research policies, see our Editorial Policies and the Editorial Policy Checklist.

Statistics

For all statistical analyses, confirm that the following items are present in the figure legend, table legend, main text, or Methods section.

n/a	Confirmed	
☐	☒	The exact sample size (*n*) for each experimental group/condition, given as a discrete number and unit of measurement
☐	☒	A statement on whether measurements were taken from distinct samples or whether the same sample was measured repeatedly
☐	☒	The statistical test(s) used AND whether they are one- or two-sided *Only common tests should be described solely by name; describe more complex techniques in the Methods section.*
☒	☐	A description of all covariates tested
☐	☒	A description of any assumptions or corrections, such as tests of normality and adjustment for multiple comparisons
☐	☒	A full description of the statistical parameters including central tendency (e.g. means) or other basic estimates (e.g. regression coefficient) AND variation (e.g. standard deviation) or associated estimates of uncertainty (e.g. confidence intervals)
☐	☒	For null hypothesis testing, the test statistic (e.g. *F*, *t*, *r*) with confidence intervals, effect sizes, degrees of freedom and *P* value noted *Give P values as exact values whenever suitable.*
☒	☐	For Bayesian analysis, information on the choice of priors and Markov chain Monte Carlo settings
☒	☐	For hierarchical and complex designs, identification of the appropriate level for tests and full reporting of outcomes
☐	☒	Estimates of effect sizes (e.g. Cohen's *d*, Pearson's *r*), indicating how they were calculated

Our web collection on statistics for biologists contains articles on many of the points above.

Software and code

Policy information about availability of computer code

Data collection	Excel version 16.36 (Microsoft) was used for dataset collection and management. Softmax Pro versions 4.3 and 7.1 (Molecular Devices) were used for HbAlc, total protein, and BODI PY assay measurements. Xcalibur software (ThermoFisher) was used to perform automated lipid detection with shotgun lipidomics. Targetlynx version 4.2 (Waters Corporation) was used for channel detection and smoothing for total tissue lipids. EZ-Cl version 3.80 (Nikon) was used for confocal image acquisition. Image Studio version 3.0 (LI-COR) was used for western blot image acquisition. NanoDrop 2000 software version 1.6.198 (ThermoFisher) was used to measure RNA concentrations and purities. 7500 software version 2.0.5. (Applied Biosystems) was used for qPCR. REDCap version 9.5.22 was used to collect clinical data from study participants.
Data analysis	Excel version 16.36 (Microsoft) was used for dataset compilation. Spike2 version 8.14 (Cambridge Electronic Design) for template-matching and quantification of single-fiber electrophysiology recordings. Targetlynx (Waters Corporation) was used for channel integration and quantification of total lipids. FIJI version 2.0 for image analysis. Image Studio version 3.0 (LI-COR) was used for western blot densitometry. Prism version 9.0 (GraphPad) was used for statistical analyses and data visualization. OmniGraffle version 7.18.1 (The Omni Group) for illustrations and figure organization.

For manuscripts utilizing custom algorithms or software that are central to the research but not yet described in published literature, software must be made available to editors and reviewers. We strongly encourage code deposition in a community repository (e.g. GitHub). See the Nature Research guidelines for submitting code & software for further information.

Data

Policy information about availability of data

All manuscripts must include a data availability statement. This statement should provide the following information, where applicable:

- Accession codes, unique identifiers, or web links for publicly available datasets
- A list of figures that have associated raw data
- A description of any restrictions on data availability

Provide your data availability statement here.

Field-specific reporting

Please select the one below that is the best fit for your research. If you are not sure, read the appropriate sections before making your selection.

☒ Life sciences ☐ Behavioural & social sciences ☐ Ecological, evolutionary & environmental sciences

For a reference copy of the document with all sections, see nature.com/documents/nr-reporting-summary-flat.pdf

Life sciences study design

All studies must disclose on these points even when the disclosure is negative.

Sample size	Power analysis has been conducted previously for similar preclinical experiments using G*Power version 3.1 (available at: https://www.psychologie.hhu.de/arbeitsgruppen/allgemeine-psychologie-und-arbeitspsychologie/gpower.html). Experiments were powered to 80% for detecting a 25% effect (2-sided test at P<0.05 using variances from our previous studies).
Data exclusions	Mice that died during the course of an experimental paradigm were excluded from analysis.
Replication	Experimental replicates are primarily described in the figure legends. Behavioral experiments were replicated at least twice using mice from separate diet cohorts. Ex vivo technical replicates were run in at least triplicate with 3 or more biological replicates.
Randomization	After 1 week of acclimation, mice were randomized into diet groups. For the clinical study, participants were placed in either control or diabetic group based on clinical diagnosis.
Blinding	Behavioral experiments were blinded by separate lab personnel, including observation box randomization and treatment allocation. Behavioral experiments involving naive db/db mice were not blinded due to obvious phenotype compared to WT or diet mice. Confocal images were numerically coded for blinding prior to image analysis. Tissues, homogenates, extracts collected for testing were generally coded to maintain blinding. De-identified patient samples were fully processed through HPLC-MS/MS and analysis before un-blinding of group allocation.

Reporting for specific materials, systems and methods

We require information from authors about some types of materials, experimental systems and methods used in many studies. Here, indicate whether each material, system or method listed is relevant to your study. If you are not sure if a list item applies to your research, read the appropriate section before selecting a response.

Materials & experimental systems

n/a	Involved in the study
☐	☒ Antibodies
☒	☐ Eukaryotic cell lines
☒	☐ Palaeontology and archaeology
☐	☒ Animals and other organisms
☐	☒ Human research participants
☒	☐ Clinical data
☒	☐ Dual use research of concern

Methods

n/a	Involved in the study
☒	☐ ChIP-seq
☒	☐ Flow cytometry
☒	☐ MRI-based neuroimaging

Antibodies

Antibodies used

Confocal Microscopy:
Polyclonal Rabbit Anti-PGP9.5 IgG (1:1000 from stock; AB1761-1, Millipore)
Monoclonal Rabbit Anti-ATF3 IgG [EPR19488] (1:400 from stock; ab207434, Abcam)
Polyclonal Chicken Anti-NeuN IgY (1:500 from stock; ABN91, Millipore)
Polyclonal Chicken Anti-NFH IgY (1:5000 from stock; 822601, Biolegend)
Polyclonal Guinea Pig Anti-TRPVl IgG (1:700 from stock; GP14100, Neuromics)

Polyclonal Rabbit Anti-PLA2g7 IgG (1:500 from stock; 15526-1-AP, ProteinTech)
Polyclonal Goat Anti-GFRA2 IgG (1:500 from stock; AF429, R&D Systems)
Polyclonal Rabbit Anti-Ibal IgG (1:1500 from stock; 019-19741, Wako Chemicals)
Polyclonal Guinea Pig Anti-c-Fos IgG (1:700 from stock; 226004, Synaptics Systems)
Isolectin GS-IB4 Alexa Fluor® 488 Conjugate (1:800 from stock; 121411, ThermoFisher)
Alexa Fluor® 488 AffiniPure Donkey Anti-Chicken IgY (IgG) (H+L) (1:500 from stock; 703-545-155, Jackson ImmunoResearch)
Alexa Fluor® 488 AffiniPure Donkey Anti-Rabbit IgG (H+L) (1:500 from stock; 711-545-152, Jackson ImmunoResearch)
Alexa Fluor® 647 AffiniPure Donkey Anti-Guinea Pig IgG (H+L) (1:500 from stock; 706-605-148, Jackson ImmunoResearch)
Rhoda mine Red-X AffiniPure Donkey Anti-Goat IgG (H+L) (1:500 from stock; 705-295-147, Jackson ImmunoResearch)
Alexa Fluor® 568 Donkey Anti-Rabbit IgG (H+L) (1:500 from stock; A10042, Thermo Fisher)

Western Blotting:
Polyclonal Rabbit Anti-PLA2g7 IgG (1:500 from stock; 15526-1-AP, ProteinTech)
Monoclonal Mouse Anti-GAPDH IgG (1:1000 from stock; sc-32233, Santa Cruz)
IRDye® 800CW Donkey Anti-Rabbit IgG (1:10,000 from stock; 926-32213, LI-COR Biosciences)
IRDye® 680RD Donkey Anti-Mouse IgG (1:10,000 from stock; 926-68072, LI-COR Biosciences)

Validation

Antibodies used in this study are commercially available and have been validated by their corresponding manufacturers (see below). Dilution factors were further optimized in the laboratory by testing multiple dilutions on the target tissues of interest.
Polyclonal Rabbit Anti-PGP9.5 IgG - https://www.emdmillipore.com/US/en/product/ Anti-Protein-Gene-Product-9.5-Antibody,MM_NF-ABl761-1#
Monoclonal Rabbit Anti-ATF3 IgG [EPR19488] - https://www.abcam.com/atf3-antibody-epr19488-chip-grade-ab207434.html
Polyclonal Chicken Anti-NeuN IgY- https://www.emdmillipore.com/US/en/product/Anti-NeuN-Antibody,MM_NF-ABN91
Polyclonal Chicken Anti-NFH IgY - https://www.biolegend.com/en-us/products/purified-anti-neurofilament-h-nf-h-antibody-11474
Polyclonal Guinea Pig Anti-TRPV1 IgG - https://www.neuromics.com/GP14100
Polyclonal Rabbit Anti-PLA2g7 IgG - https://www.ptglab.com/products/PLA2G7-Antibody-15526-1-AP.htm
Polyclonal Goat Anti-GFRA2 IgG - https://www.rndsystems.com/products/human-mouse-gfr-alpha-2-gdnf-r-alpha-2-antibody_af429
Polyclonal Rabbit Anti-Iba1 IgG - https://labchem-wako.fujifilm.com/us/product/detail/W0I W0l0l-1974.html
Polyclonal Guinea Pig Anti-c-Fos IgG - https://sysy.com/product/226004
Isolectin GS-IB4 Alexa Fluor® 488 Conjugate - https://www.thermofisher.com/order/catalog/product/121411#/121411
Alexa Fluor® 488 AffiniPure Donkey Anti-Chicken IgY (IgG) (H+L) - https://www.jacksonimmuno.com/catalog/products/703-545-155
Alexa Fluor® 488 AffiniPure Donkey Anti-Rabbit IgG (H+L) - https://www.jacksonimmuno.com/catalog/products/711-545-152
Alexa Fluor® 647 AffiniPure Donkey Anti-Guinea Pig IgG (H+L) - https://www.jacksonimmuno.com/catalog/products/706-605-148
Rhodamine Red-X AffiniPure Donkey Anti-Goat IgG (H+L) - https://www.jacksonimmuno.com/catalog/products/705-295-147
Alexa Fluor® 568 Donkey Anti-Rabbit IgG (H+L) - https://www.thermofisher.com/antibody/product/Donkey-anti-Rabbit-IgG-H-L-Highly-Cross-Adsorbed-Secondary-Antibody-Polyc1onal/Al0042
Monoclonal Mouse Anti-GAPDH IgG - https://www.scbt.com/p/gapdh-antibody-6c5
IRDye® 800CW Donkey Anti-Rabbit IgG - https://www.licor.com/bio/reagents/irdye-800cw-donkey-anti-rabbit-igg-secondary-antibody
IRDye® 680RD Donkey Anti-Mouse IgG - https://www.licor.com/bio/reagents/irdye-680rd-donkey-anti-mouse-igg-secondary-antibody

Animals and other organisms

Policy information about studies involving animals; ARRIVE guidelines recommended for reporting animal research

Laboratory animals	Mice utilized inlcude: Male C57BL/6J mice, 8-10 weeks of age (#000664, The Jackson Laboratory), Female C57BL/6J mice, 8-10 weeks of age (#000664, The Jackson Laboratory), and Male BKS.Cg-Dock7m+/+Leprdb/J, 16 weeks of age (db/db , #000642, The Jackson Laboratory). Mice were housed in groups of 4-5, maintained on a 12-hour light–dark cycle with ambient temperatures between 20 and 22° C, and with free access to food and water.
Wild animals	Wild animals were not used in this study.
Field-collected samples	There were no field-collected samples in this study.
Ethics oversight	All animal experiments conformed to the Guidelines for the Use of Animals in Research as put forward by the International Association for the Study of Pain, and to protocols approved by the University of Texas Health Science Center at San Antonio Institutional Animal Care and Use Committee.

Note that full information on the approval of the study protocol must also be provided in the manuscript.

Human research participants

Policy information about studies involving human research participants

Population characteristics	Sixteen subjects with a medical diagnosis of painful diabetic neuropathy were enrolled (age range 57-84, 8 males, 8 females), along with twelve non-diabetic subjects to serve as age-matched controls (age range 56-93, 6 males, 6 females). Additional data are found in Supplementary Table 2. Diagnostic criteria for diabetic neuropathy included the presence of two or more symptoms or signs: (1) neuropathic symptoms (e.g., decreased sensation, "asleep numbness", prickling, stabbing, burning, or aching pain) predominantly in the toes, feet, or legs; (2) decreased distal sensation or unequivocally decreased (or absent) ankle reflexes; (3) validated abnormalities based on nerve conduction studies.
Recruitment	The primary sources of accrual were clinician referrals to the study coordinator or responses to I RB-approved advertisements posted in the outpatient neurology clinic. Interested patients were introduced to the study coordinator, who

	presented the study and addressed all questions or concerns prior to formal written consent for study entry. Confirmation of the diagnosis of diabetic polyneuropathy was based on available medical records that were reviewed after informed consent was obtained. Recruitment of age-matched control subjects occurred through referrals from family or friends of study participants, and through the advertisements posted. To minimize introduction of bias, clinically-relevant demographics were withheld until laboratory sample processing was completed.
Ethics oversight	Regulatory approval was obtained from the Human Subjects Institutional Review Board at the University of Texas Health Science Center at San Antonio (#20160027HU).

Note that full information on the approval of the study protocol must also be provided in the manuscript.